Experimental methods for studies of ion – molecule reaktions and of ion – electron rekombination

Time dependence of the value of recombination rate coefficient for H_3^+ ions with electrons

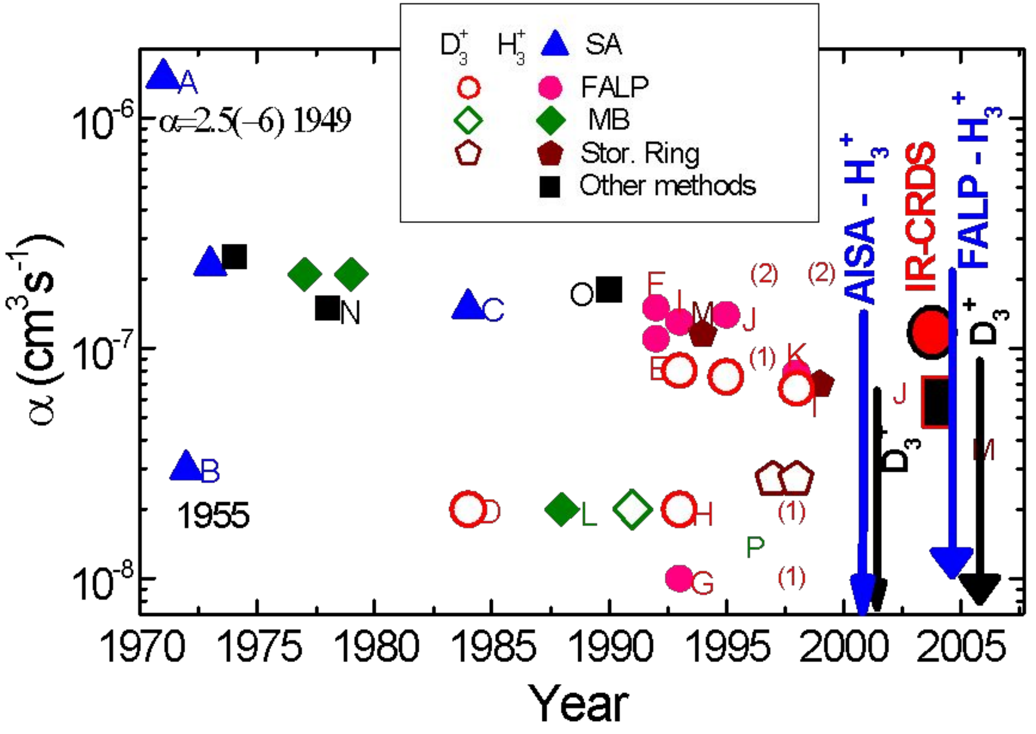

A – M.A. Biondi
B – K.B. Persson
C – J.A. Mac Donald
D – N.G. Adams
E,F – A. Canosa
H,G,I – D. Smith
J – T. Gougousi
K – S. Laube
L – H. Hus
M – M. Larson
N – D. Mathur
O – T. Amano
P – P. Van der Donk
(1) – $v=0$
(2) – $v>0$

Not a simple problem

$$H_3^+ + e^- \xrightarrow{\alpha_{\text{bin}}} H + H + H,\ H_2 + H$$

Different experiments

Ion Storage Ring

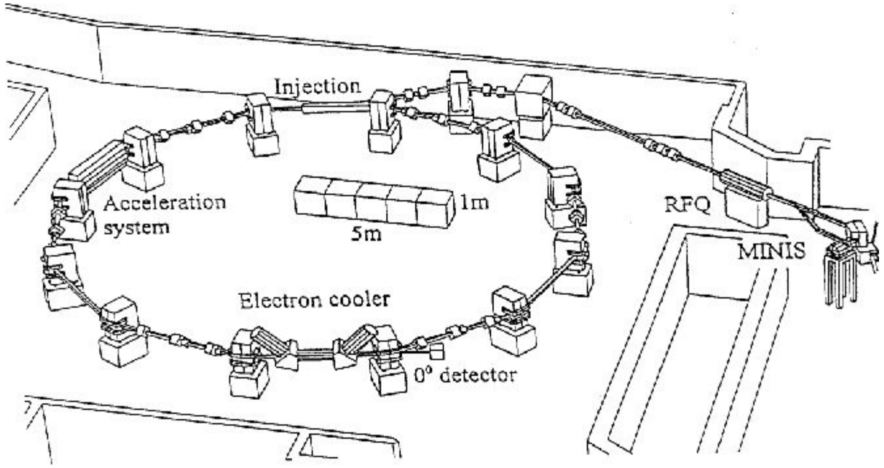

- \+ No buffer gas
- \+ Excellent energy resolution

- \- Complicated estimation of cross section from measured data
- \- Rotational temperature of ions in the ring can be >= 300 K

Afterglow plasma

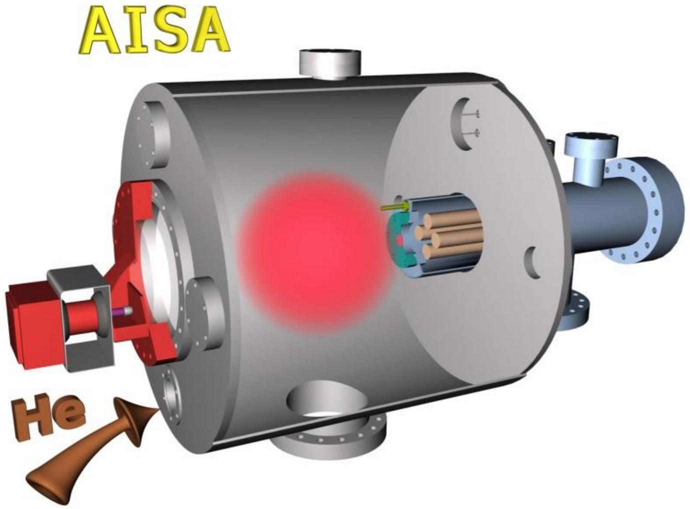

- \+ Many collisions of ions with buffer gas particles – effective thermalization
- \+ The measured quantity is thermal rate coefficient

- \- Complicated chemical kinetics
- \- Presence of third bodies can influence the recombination

Ion storage ring

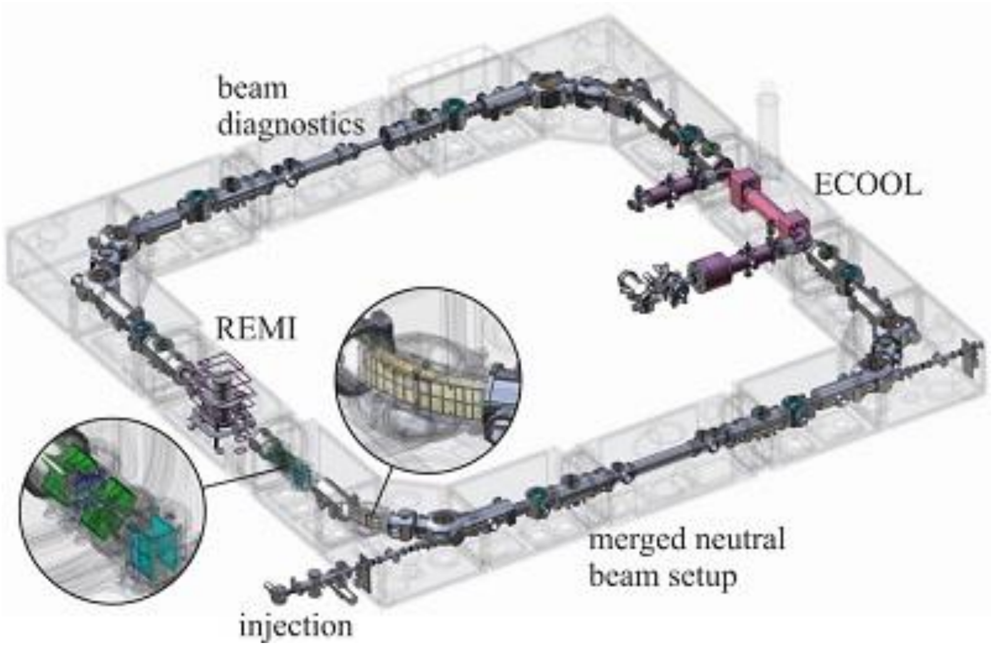

Figure 1: Design model of the CSR showing the electrostatic ion optical elements (enlarged in circuits), the injection line, the electron cooler (straight section at the right side) and the reaction microscope (straight section at the left side)

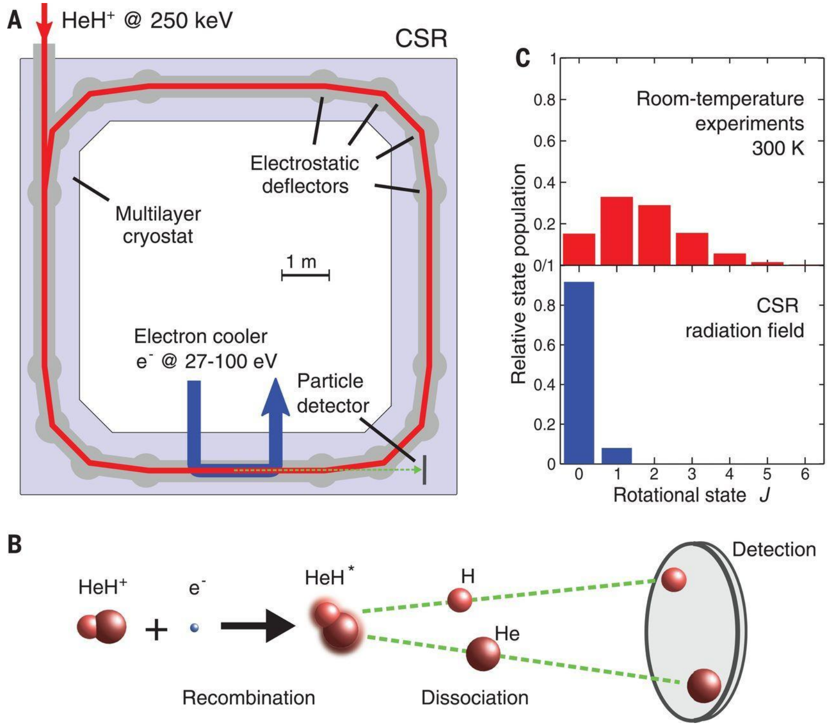

(A) Scheme of the CSR ring structure with the injected and stored HeH^+ ion beam (red), merged electron beam (blue), reaction products (green), and particle detector. (B) Reaction scheme and position-sensitive detection of coincident fragments. (C) Equilibrium rotational state populations of HeH+ for previous studies (300 K) and the estimated radiation field in the CSR.

Recombination of ions in specific quantum state

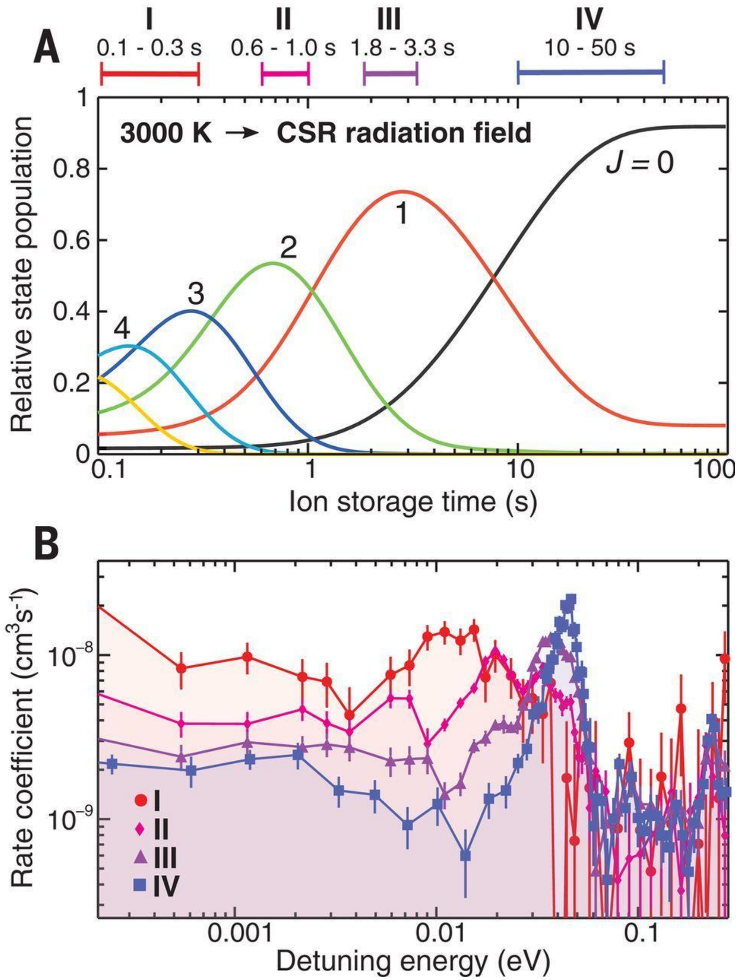

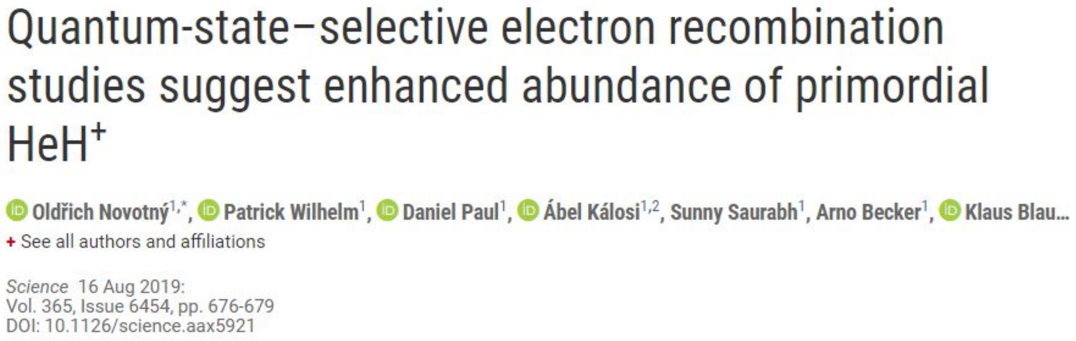
Quantum-state–selective electron recombination studies suggest enhanced abundance of primordial HeH^+

Oldřich Novotný[1,*], Patrick Wilhelm[1], Daniel Paul[1], Ábel Kálosi[1,2], Sunny Saurabh[1], Arno Becker[1], Klaus Blau...

+ See all authors and affiliations

Science 16 Aug 2019:
Vol. 365, Issue 6454, pp. 676-679
DOI: 10.1126/science.aax5921

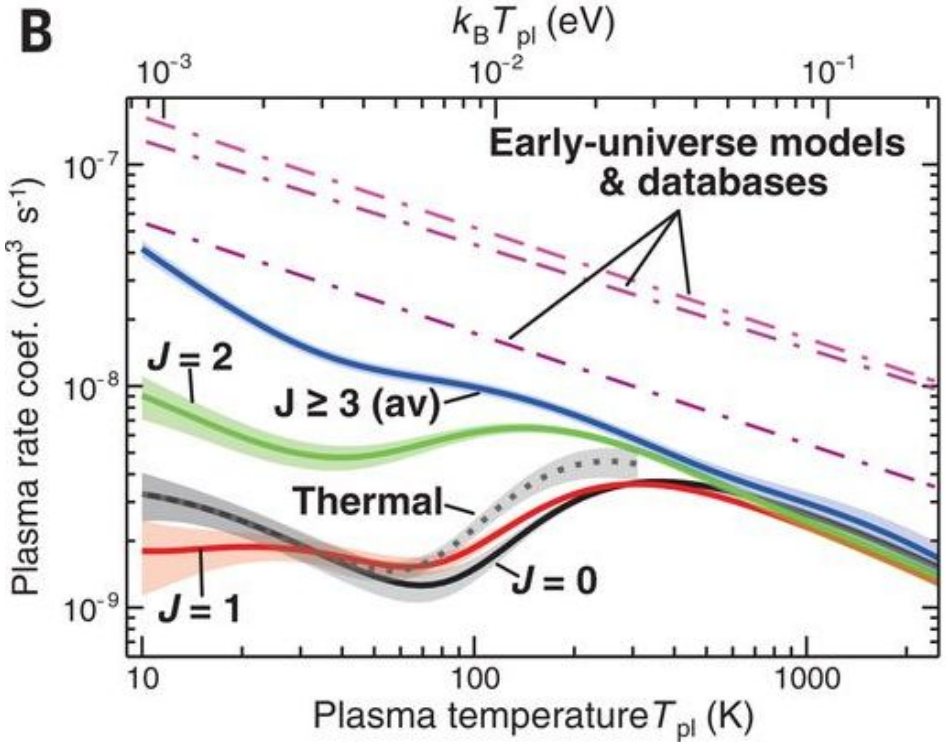

Rekombination of H_3^+ ions with electrons

Neutral assisted ternary recombination:

$$\mathrm{H}_3^+ + e^- + \mathrm{He} \xrightarrow{K_{\mathrm{He}}} neutral\ \ products$$

$$\mathrm{H}_3^+ + e^- + \mathrm{H}_2 \xrightarrow{K_{\mathrm{H2}}} neutral\ \ products$$

Electron assisted ternary recombination:

$$\mathrm{H}_3^+ + e^- + e^- \xrightarrow{K_{\mathrm{CRR}}} e^- + neutral\ \ products$$

Formation of H_5^+ and its subsequent recombination with electrons:

$$\mathrm{H}_3^+ + \mathrm{H}_2 + \mathrm{He} \xrightarrow{k_3} \mathrm{H}_5^+ + \mathrm{He}$$

$$\mathrm{H}_5^+ + e^- \xrightarrow{\alpha_5} neutral\ \ products$$

$$\alpha_{\mathrm{eff}} = \alpha_{\mathrm{bin}} + \alpha_{\mathrm{F}} \frac{K_{\mathrm{He}}[\mathrm{He}] + K_{\mathrm{H2}}[\mathrm{H}_2]}{\alpha_{\mathrm{F}} + K_{\mathrm{He}}[\mathrm{He}] + K_{\mathrm{H2}}[\mathrm{H}_2]} + \alpha_5 K_{\mathrm{C}}[\mathrm{H}_2] + K_{\mathrm{CRR}} n_{\mathrm{e}}$$

Glosík J., Dohnal P. et al., Plasma Sources Sci. Technol. 24(6), 065017, 2015

Stationary afterglow plasma

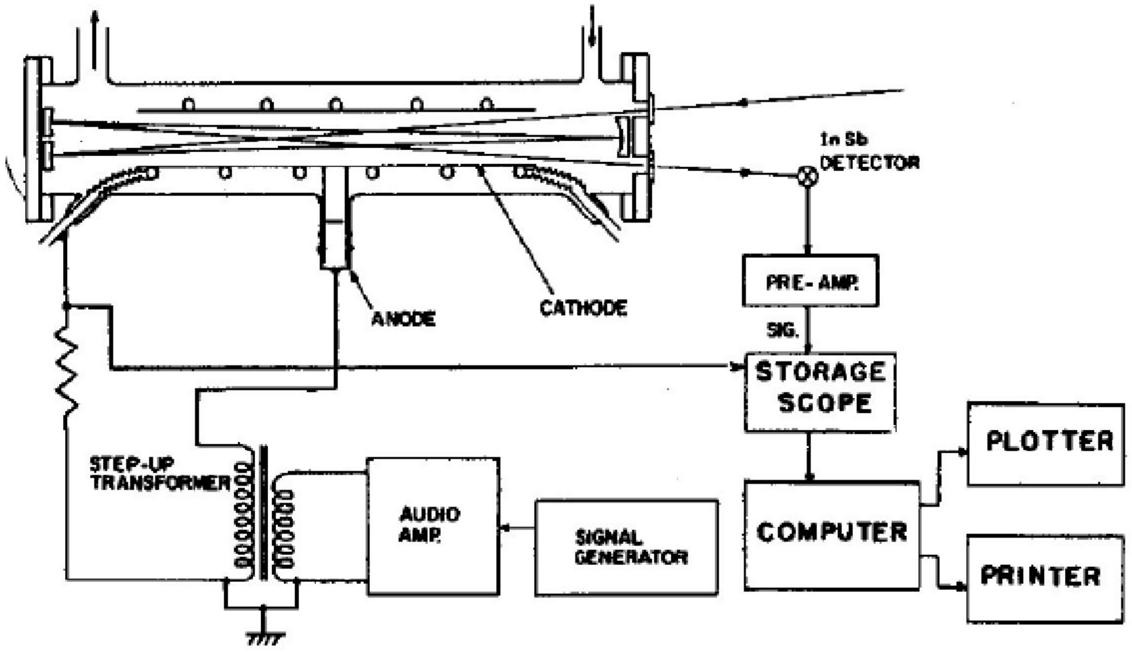

FIG. 1. A schematic diagram of the spectrometer system.

J. Chem. Phys., Vol. 92, No. 11, 1 June 1990

Combination of Stationary afterglow and absorption spectroscopy

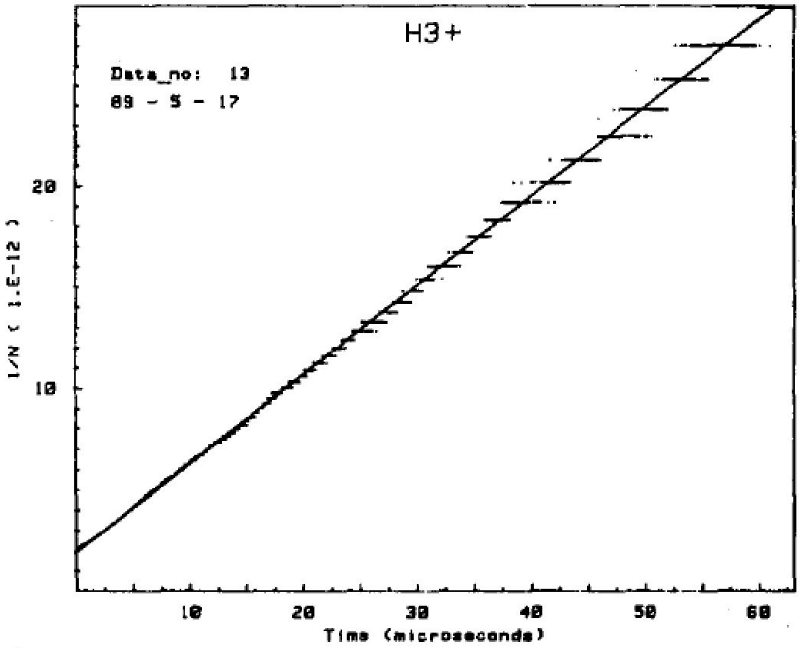

Stationary afterglow plasma

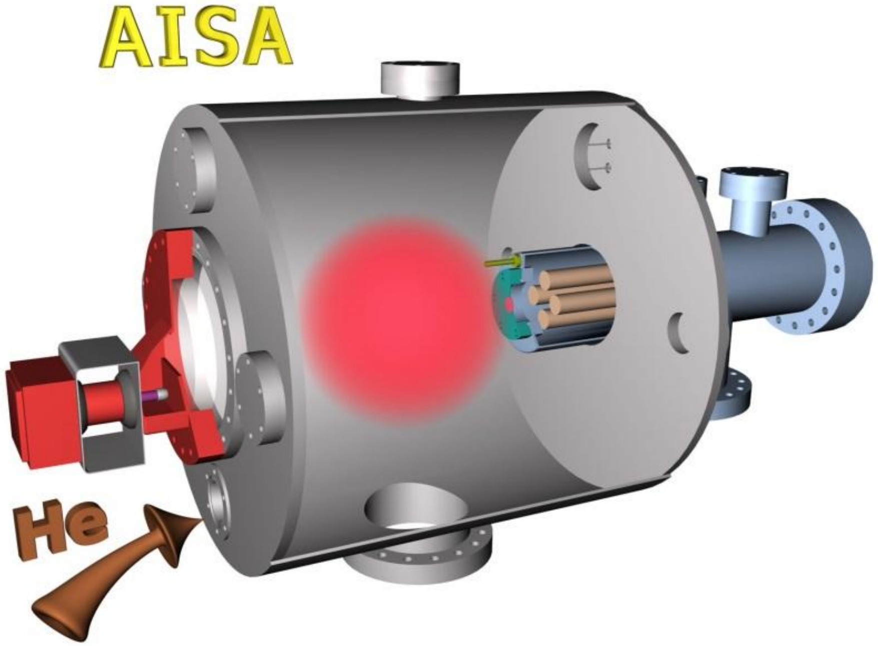

AISA – Advanced Integrated Stationary Afterglow

Mass spectrometer + Langmuir probe diagnostics

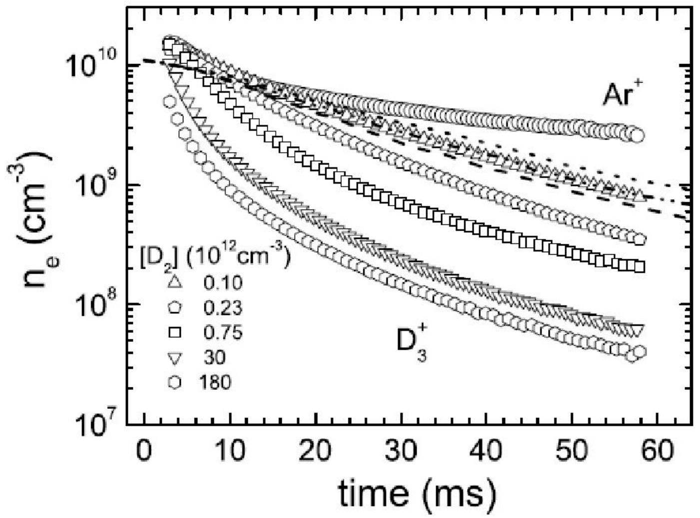

FIG. 1. Decay curves. Measured decay curves, $n_e(t)$, in D_3^+ dominated afterglow for several $[D_2]$ and 2 Torr of He. Also plotted is the decay curve for Ar^+. The dotted, dash-dot-dotted, and dashed lines indicate decays obtained from the model for $[D_2] = 1 \times 10^{11}$ cm^{-3} when using for α the values (5, 6.5, and 10) × 10^{-9} cm^3 s^{-1}, respectively.

Phys. Rev. Lett., 88 (4): Art. No. 044802 (4 pages), 2002.

Stationary afterglow plasma

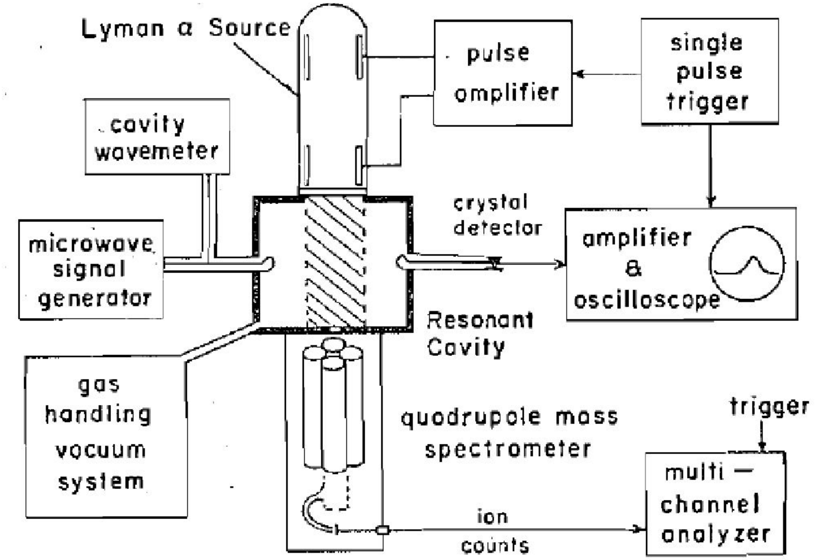

FIG. 1. Schematic diagram of a typical microwave afterglow apparatus employing mass analysis of the ions undergoing electron–ion recombination. In this case a photoionizing source is used to ionize the gas.

Microwave diagnostics + mass spectrometry

Canadian Journal of Chemistry, 47, 1711 (1969)

Microwave diagnostics of plasma

Plasma conductivity

$$\sigma = ne^2(\nu/\omega - \mathrm{j})\,(m\omega)^{-1}$$

Change of resonant frequency and resonator quality:

$$\Delta\omega_0/\omega_0 = -(2\pi/\omega_0)\left(\int_{V'} \sigma_i E^2\,\mathrm{d}V\right)\left(\int_{V'} E^2\,\mathrm{d}V\right)^{-1},$$

$$\Delta(Q^{-1}) = (4\pi/\omega_0)\left(\int_{V'} \sigma_r E^2\,\mathrm{d}V\right)\left(\int_{V} E^2\,\mathrm{d}V\right)^{-1},$$

Plasma frequency

$$\omega_{\mathrm{pe}} = \sqrt{\frac{n_{\mathrm{e}} e^2}{m^* \varepsilon_0}}$$

Microwave diagnostics of plasma

From the shift of resonant frequency we can get electron number density

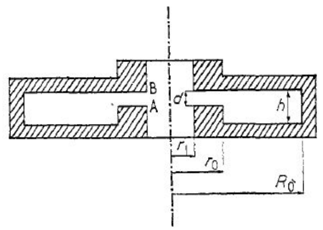

Toroidal resonator cross section. A, B, pole lengthening heads.

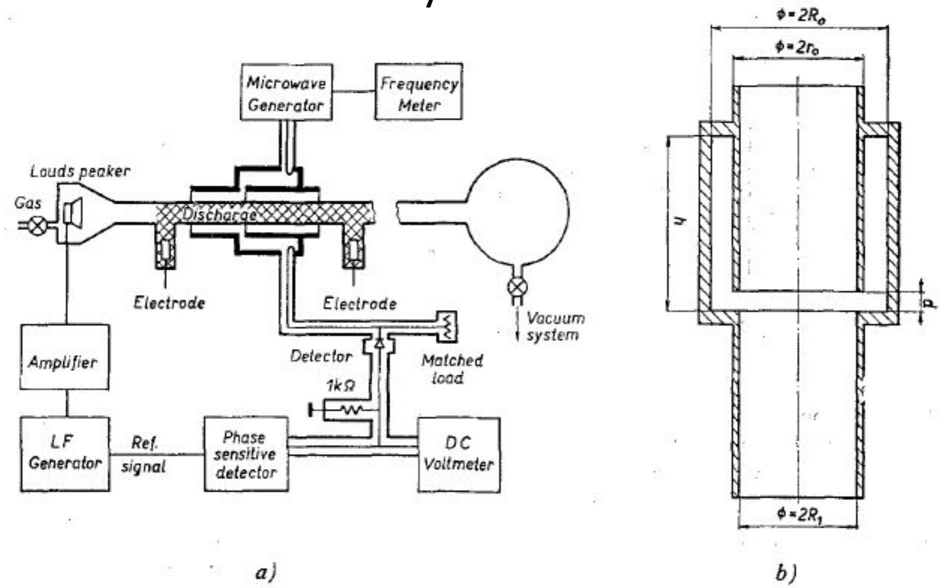

Fig. 3. *a* — Experimental arrangement. *b* — Section and dimensions of the toroidal resonator $R_0 = 4{\cdot}69$ cm, $r_0 = 3{\cdot}81$ cm, $R_1 = 3{\cdot}64$ cm, $h = 7{\cdot}0$ cm, $d = 0{\cdot}5$ cm, resonance frequency $f_0 \simeq 905$ MHz.

$$N_e(0) = \Delta f_r f_r \frac{2\pi m_e}{e_0^2} \frac{\int_v E^2 dv}{\int_{v'} I_0\left(\frac{2{\cdot}405}{r_1} r\right) E^2 dv}$$

Sicha et al., Czech. J. Phys. B 20, 684, 1970

Microwave diagnostics of plasma

- Electron number density measurement

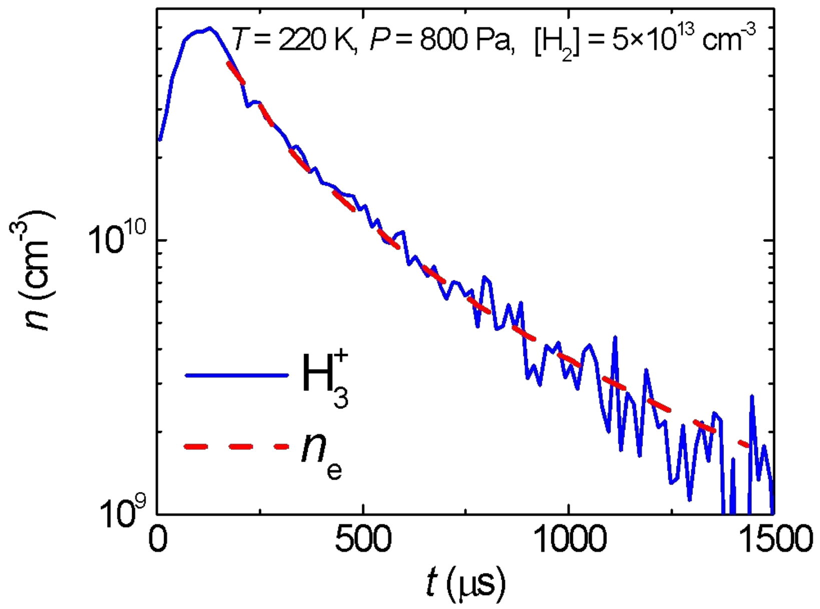

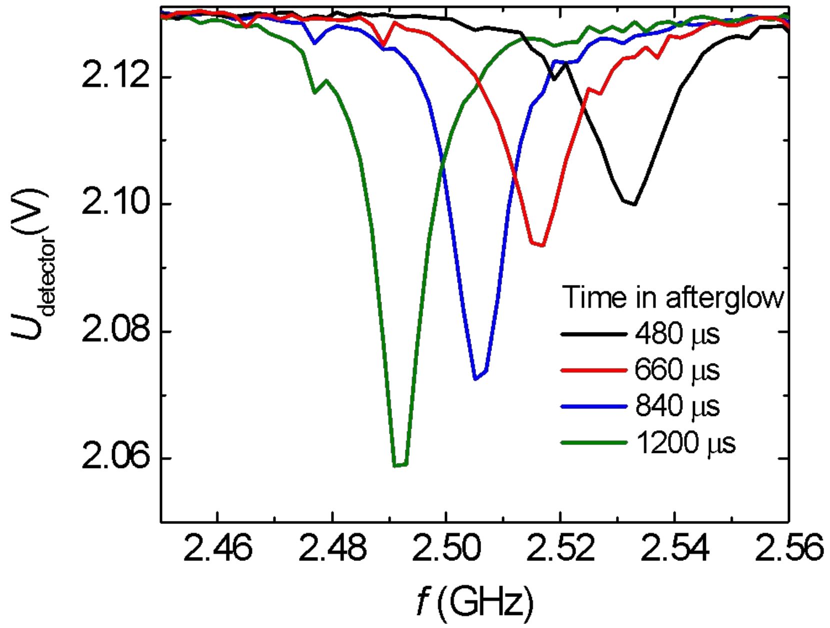

SA-CRDS apparatus

- CRDS – Cavity Ring Down Spectroscopy
- SA – Stationary Afterglow

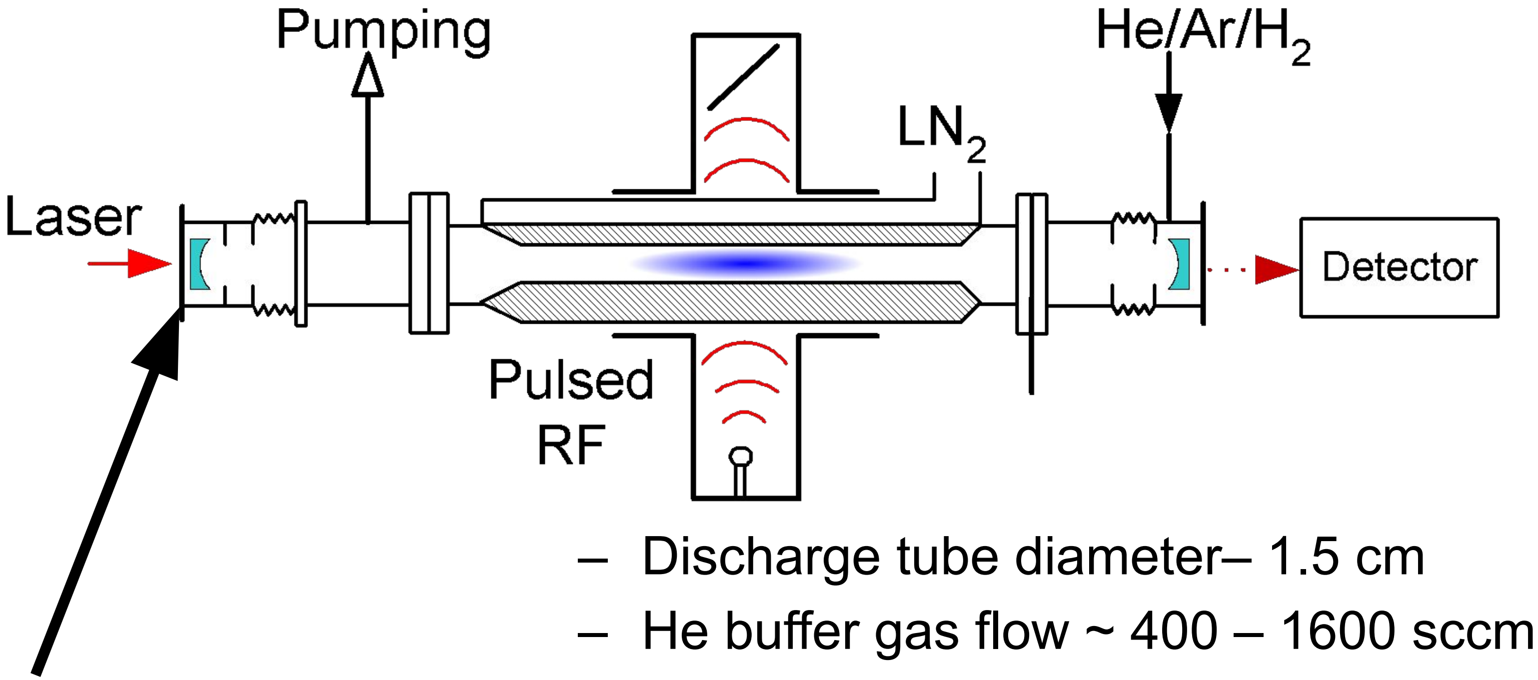

Highly reflective mirror

- Discharge tube diameter– 1.5 cm
- He buffer gas flow ~ 400 – 1600 sccm
- Pressure ~ 200 – 1500 Pa
- Temperature range ~ 77 – 300 K

Cavity ringdown spectroscopy

First used for mirror reflectivity determination (Herbelin et al. 1980).

Later, the dependence of ring-down time on absorption between the mirrors was observed (O'Keefe et al. 1988)

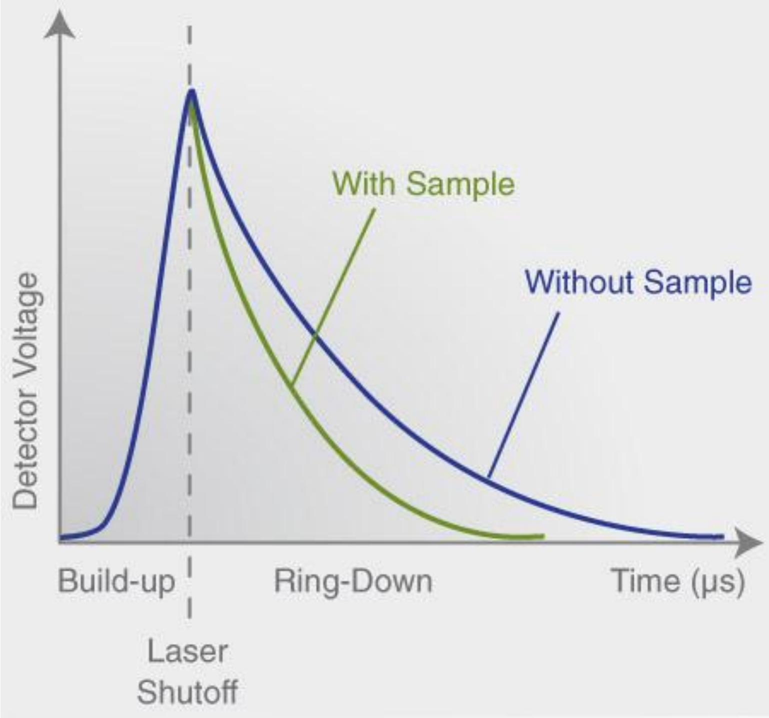

Highly reflective mirrors by Layertec (diameter 6.3 mm, reflectivity R = 99.99 %)

Herbelin et al., Appl. Opt. 19, 144, 1980.
O'Keefe et al., Rev. Sci. Instrum. 59, 2544, 1988.

SA-CRDS

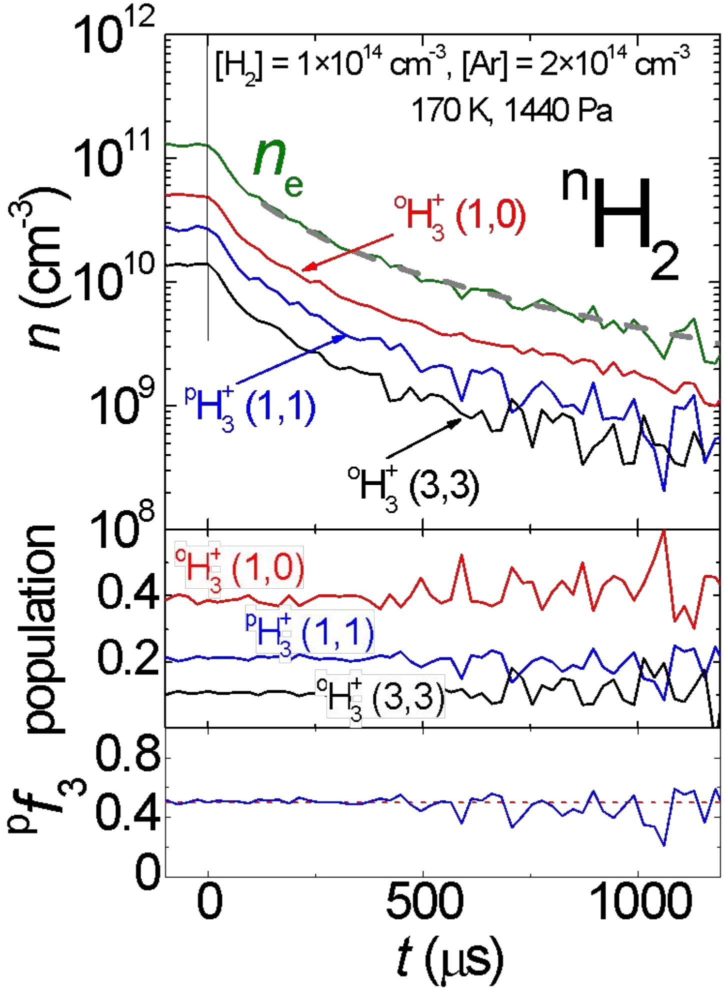

- The time evolution of ion number density is measured (of particular quantum states)
- Kinetic temperature can be determined from Doppler broadening of absorption lines
- Rotational temperature is given by relative populations of rotational states

$$\frac{\mathrm{d}n_\mathrm{e}}{\mathrm{d}t} = -\alpha_\mathrm{eff} n_\mathrm{e}^2 - \frac{1}{\tau_\mathrm{L}} n_\mathrm{e},$$

$$n_\mathrm{e}(t) = \frac{n_0}{\alpha_\mathrm{eff}\tau_\mathrm{L} n_0 \left(\exp\left(\frac{t-t_0}{\tau_\mathrm{L}}\right) - 1 \right) + \exp\left(\frac{t-t_0}{\tau_\mathrm{L}}\right)}$$

Cryo-SA-CRDS

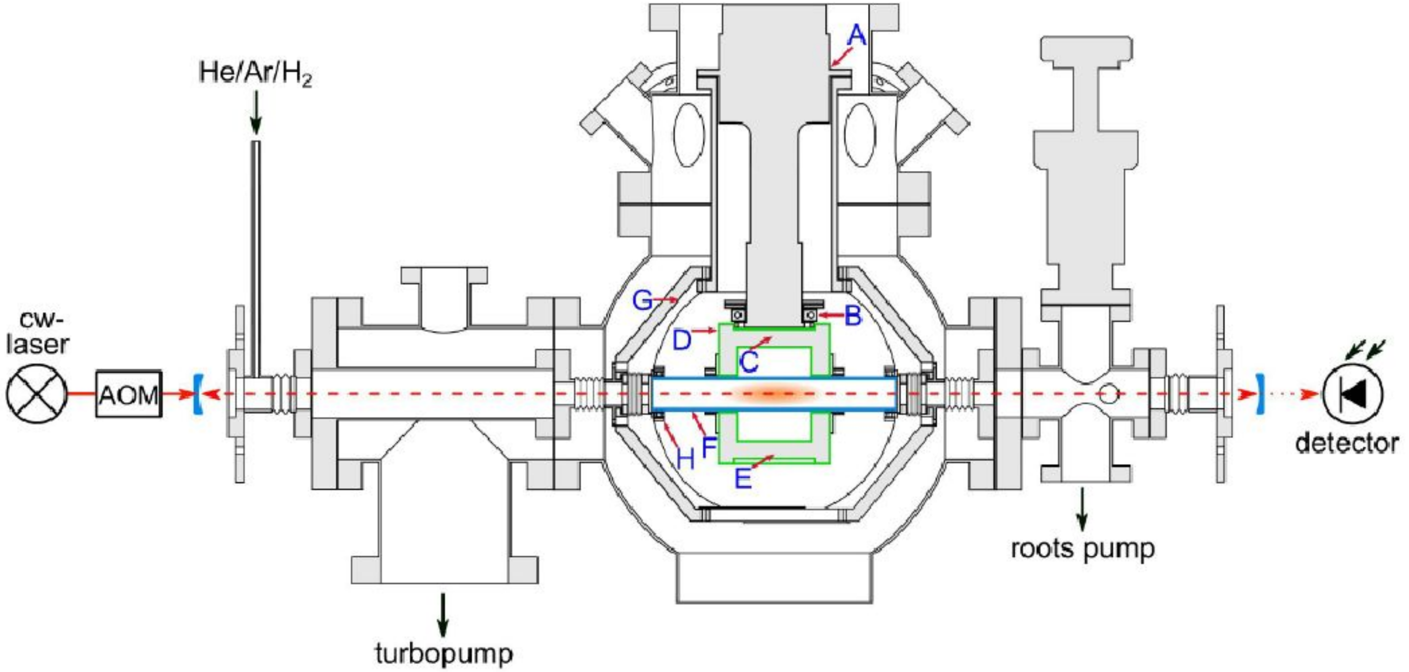

Figure 1: The Cryogenic Stationary Afterglow apparatus in conjunction with a continuous wave Cavity Ring-Down absorption Spectrometer (Cryo-SA-CRDS). Temperature sensors are denoted by blue capital letters. The discharge tube is drawn as a dark blue frame. The microwave resonator is around the tube and shown by green frame. The Sumitomo RDK 408S cold head is placed above the microwave resonator. The laser light is controlled by the acousto-optic modulator (AOM) and goes through first mirror, a discharge tube and the second mirror at the other side of the discharge tube and then to the detector.

Cryo-SA-CRDS

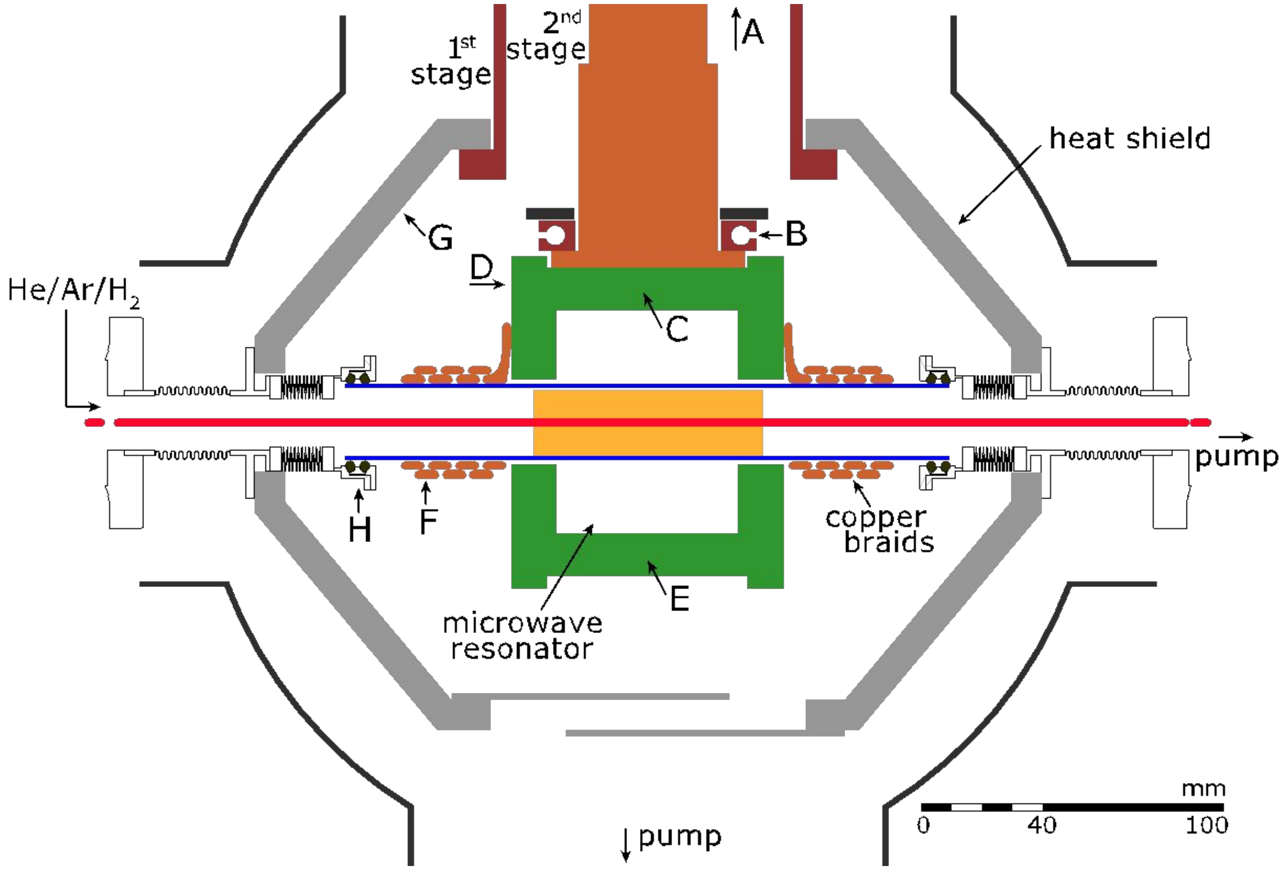
1st stage
2nd stage
A
heat shield
B
G
D
He/Ar/H2
C
pump
H
F
copper braids
E
microwave resonator
mm
0
40
100
pump

Cryo-SA-CRDS

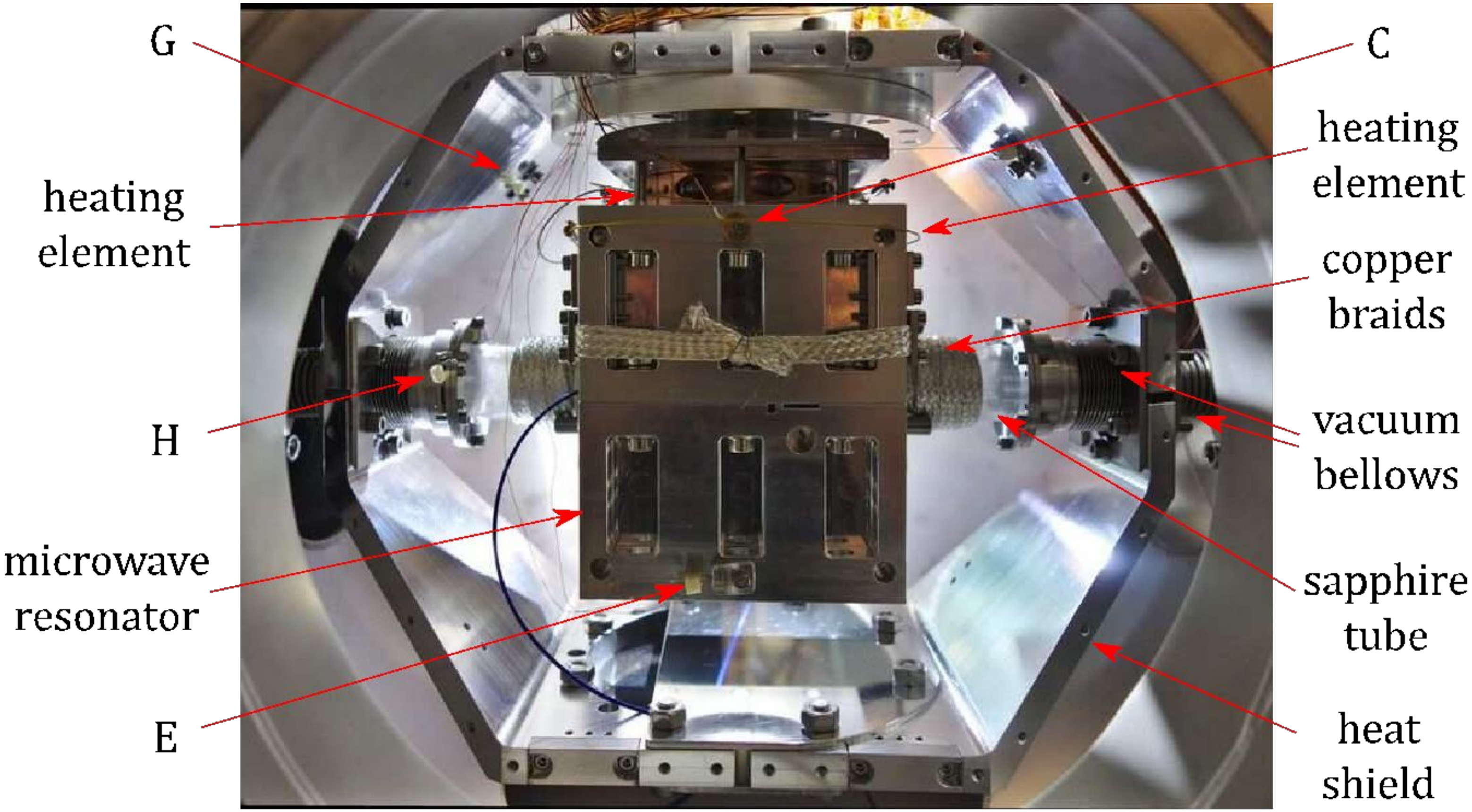

Plašil, R; Dohnal, P; Kálosi, Á; Roučka, Š; Shapko, D; Rednyk, S; Johnsen, R; Glosík, J, *Rev. Sci. Instrum.*, **89**: 063116, 2018.

H_3^+ (again)

- The lowest rotational states of the vibrational ground state

Para

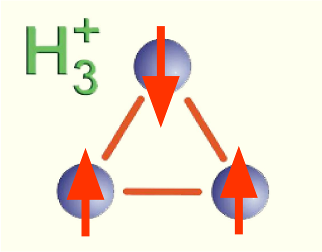

I = 1/2

Ortho

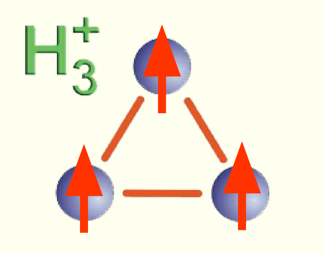

I = 3/2

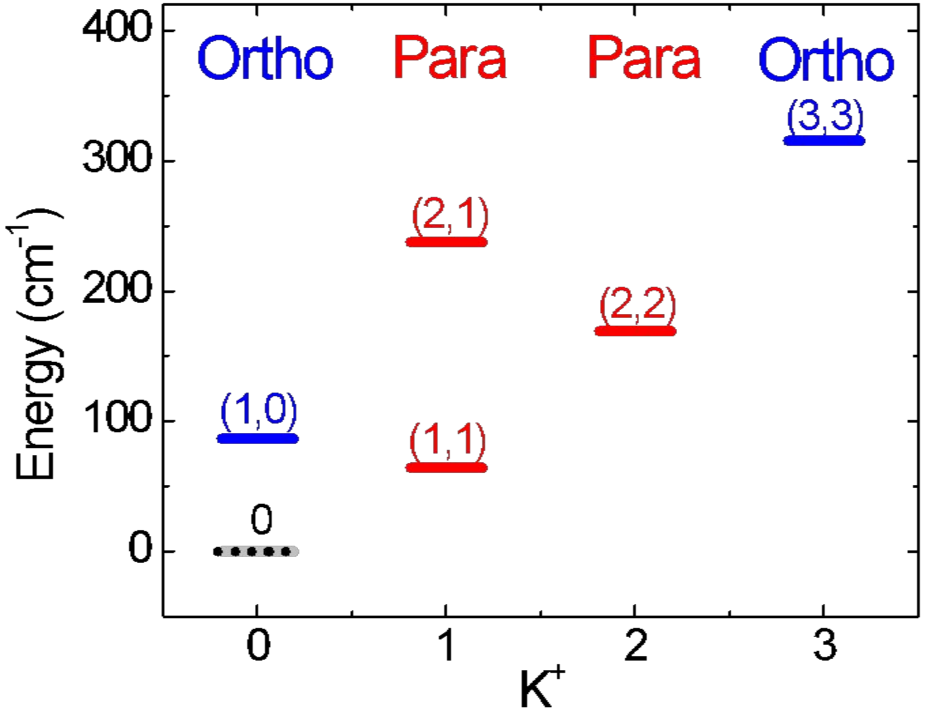

Cryo-SA-CRDS

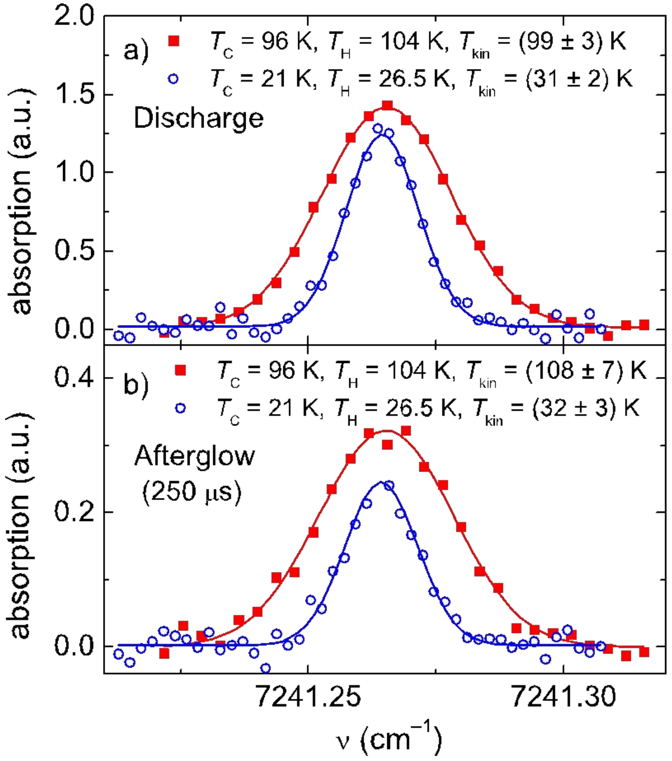

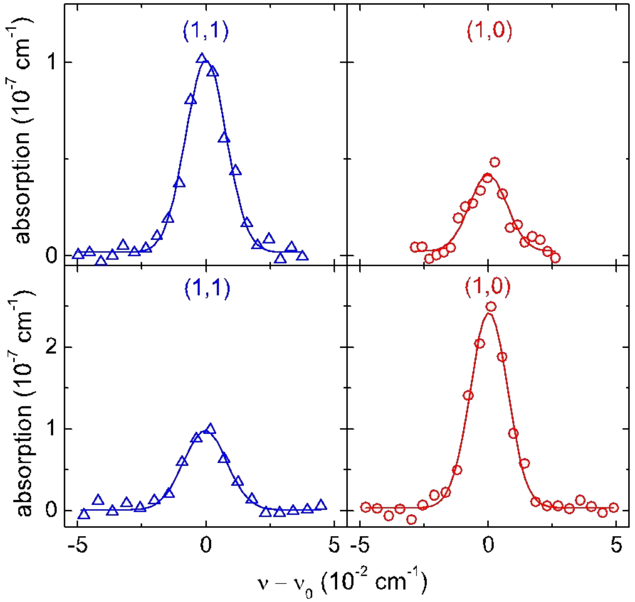

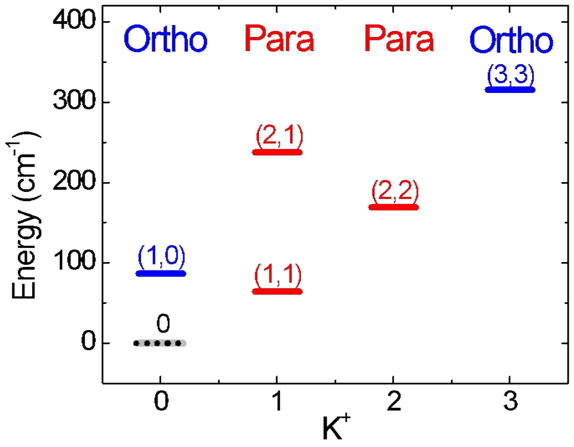

At 30 K, we can change the population of the of the lowest state of H_3^+ from 40% to 80% of all ions. The rest of the ions are mainly in the (1,0) state.

Rekombination of H_3^+ ions in specific quantum state

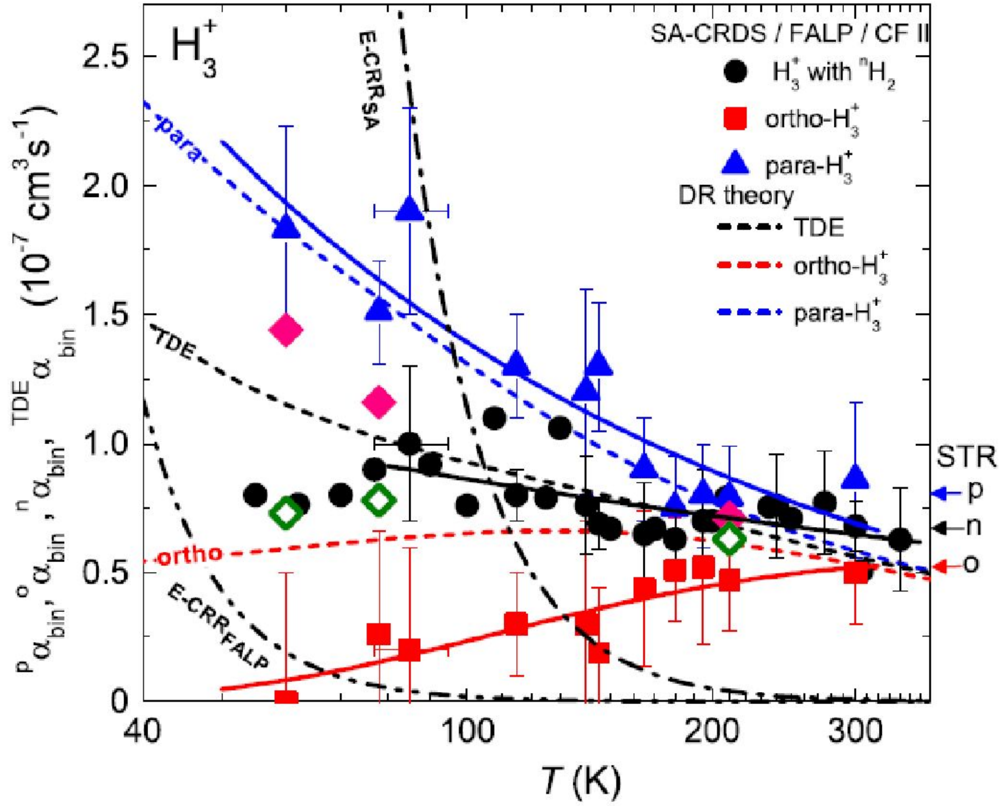

Combination of CRDS and microwave diagnostics

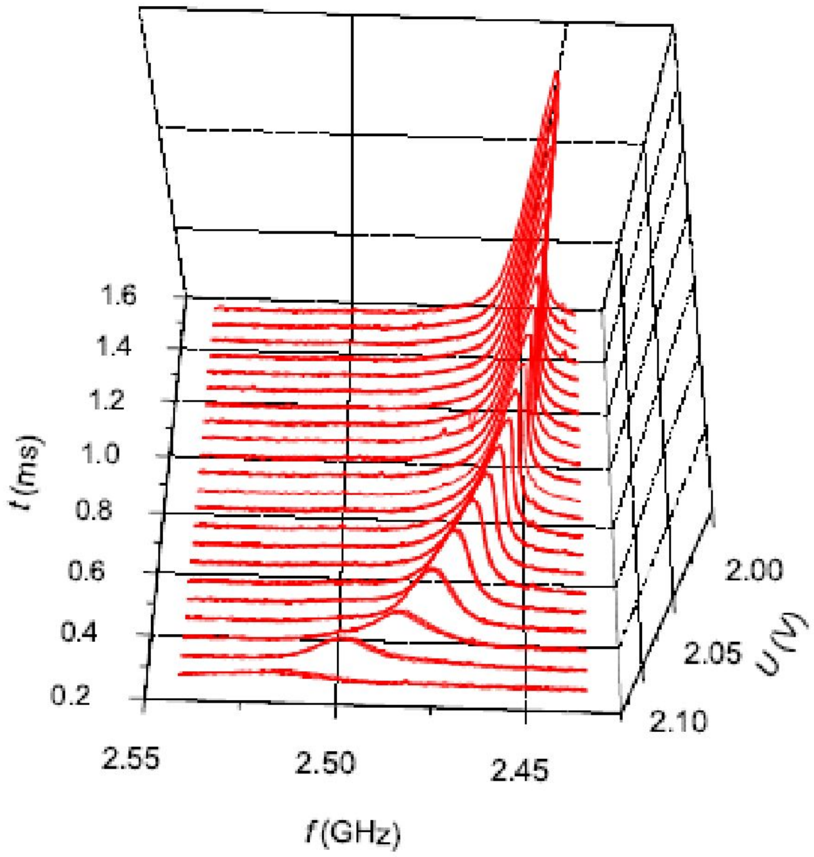

Figure 2: Time evolution of the frequency response of resonant cavity obtained in helium buffered plasma at $T = 200$ K, [He] $= 3 \times 10^{17}$ cm^{-3}, [Ar] $= 2 \times 10^{14}$ cm^{-3} and [H_2] $= 4.6 \times 10^{13}$ cm^{-3}. The frequency position of the center of each peak-like feature gives resonant frequency of the microwave resonator at a particular time in the afterglow and through equation (1) the electron number density.

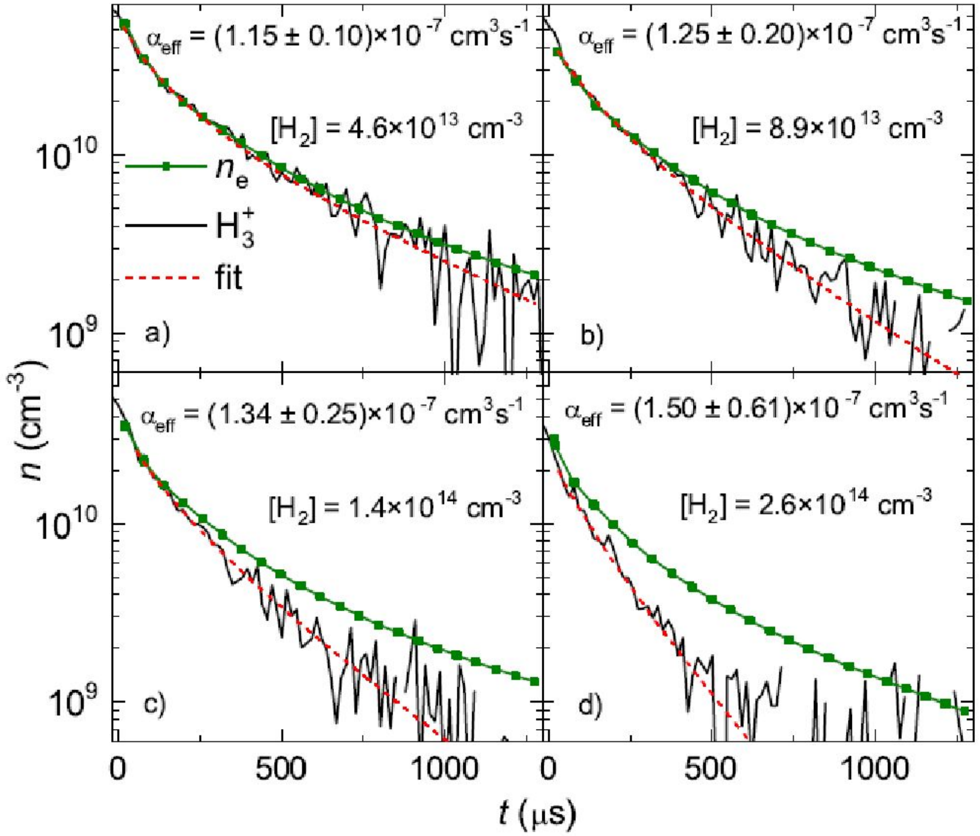

Figure 3: Measured time evolutions of the electron (squares) and H_3^+ (full line) number densities in the helium buffered afterglow plasma at different number densities of hydrogen. The dashed line denotes fit of the data using equation (9). For details on the fitting procedure see in text. The obtained effective recombination rate coefficients are written in each panel and the displayed error is the statistical error of the fit. The experiments were performed at $T = 200$ K, [He] $= 3 \times 10^{17}$ cm^{-3} and [Ar] $= 2 \times 10^{14}$ cm^{-3} with [H_2] in the range of 4.6×10^{13} to 2.6×10^{14} cm^{-3}.

Journal of Molecular Spectroscopy 378 (2021) 111450

Studied ion is not dominant in plasma

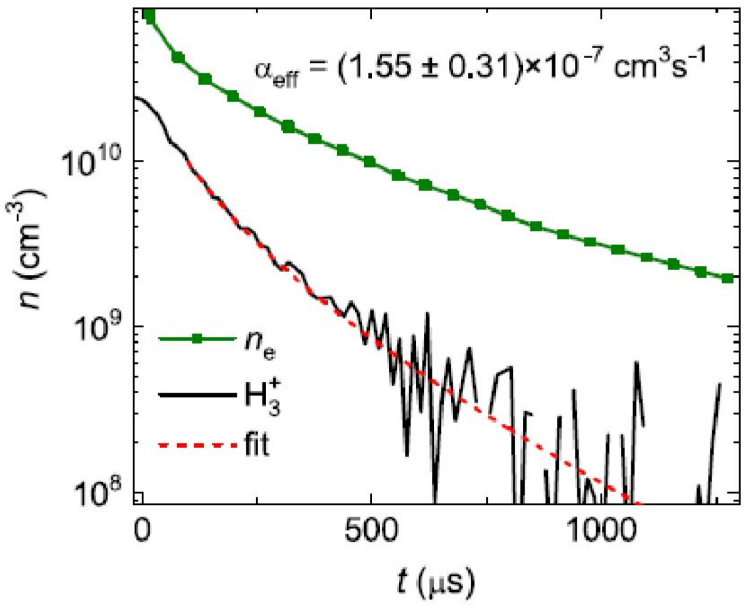

Fig. 5. Example of time evolution of electron (squares) and H_3^+ (full line) number densities measured in a neon buffered afterglow plasma at $T = 110$ K, [Ne] = 6.3×10^{17} cm^{-3}, [Ar] = 5.4×10^{13} cm^{-3}, [H_2] = 1.0×10^{14} cm^{-3}. Fit to the data using Eq. (9) is denoted by a dashed line and the obtained effective recombination rate coefficient is displayed in the figure.

$$\frac{dn_{H_3}}{dt} = -\alpha_{eff} n_{H_3} n_e - \frac{n_{H_3}}{\tau}$$

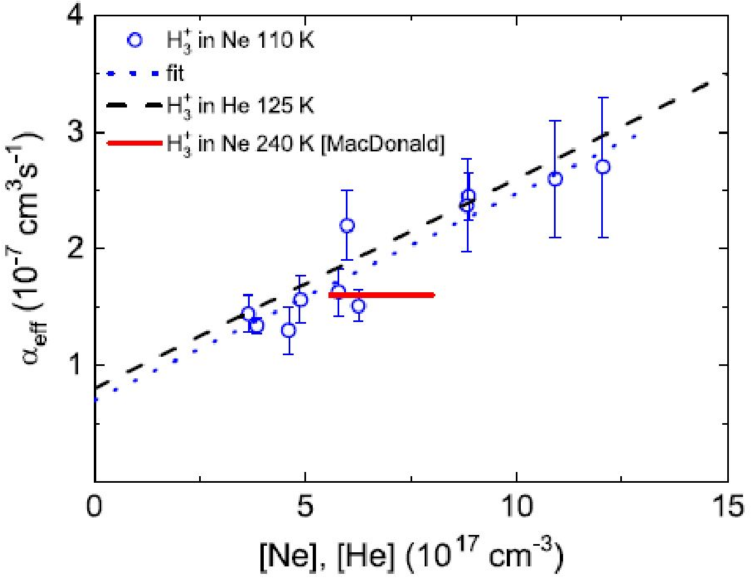

Fig. 6. The dependence of the effective recombination rate coefficients for recombination of H_3^+ ions with electrons on buffer gas number density obtained in the present study in neon buffer gas at 110 K (circles). The fit to the data by Eq. (3) is shown as a dotted line. The values are compared to those reported by Dohnal et al. [43] in helium buffer gas (dashed line) and by MacDonald et al. [31] in neon buffer gas at 240. K (full line).

$$n_{H_3}(t_i) = n_{H_3}(t_0)e^{-\alpha_{eff}X(t_i)-\frac{1}{\tau}Y(t_i)},$$

where $n_{H_3}(t_0)$ is the initial density of H_3^+ ions,

$$X(t_i) = \int_{t_0}^{t_i} n_e(t)dt,$$

and

$$Y(t_i) = t_i - t_0,$$

Flowing afterglow plasma

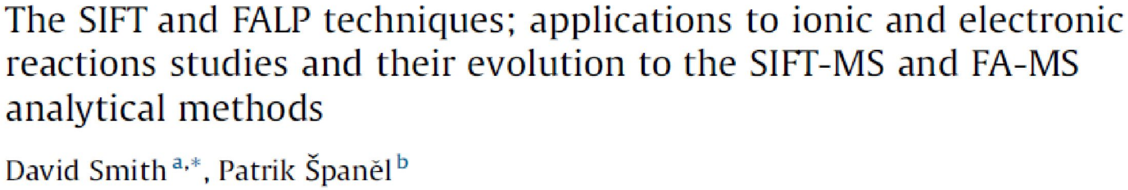

The SIFT and FALP techniques; applications to ionic and electronic reactions studies and their evolution to the SIFT-MS and FA-MS analytical methods

David Smith[a,*], Patrik Španěl[b]

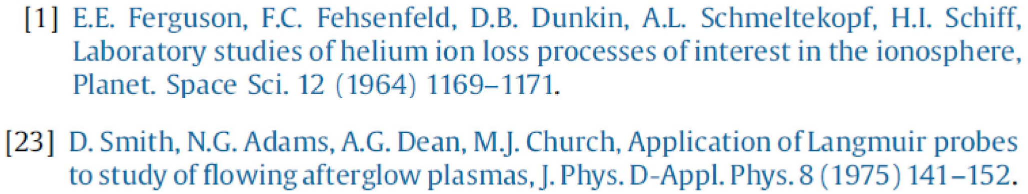

[1] E.E. Ferguson, F.C. Fehsenfeld, D.B. Dunkin, A.L. Schmeltekopf, H.I. Schiff, Laboratory studies of helium ion loss processes of interest in the ionosphere, Planet. Space Sci. 12 (1964) 1169–1171.

[23] D. Smith, N.G. Adams, A.G. Dean, M.J. Church, Application of Langmuir probes to study of flowing afterglow plasmas, J. Phys. D-Appl. Phys. 8 (1975) 141–152.

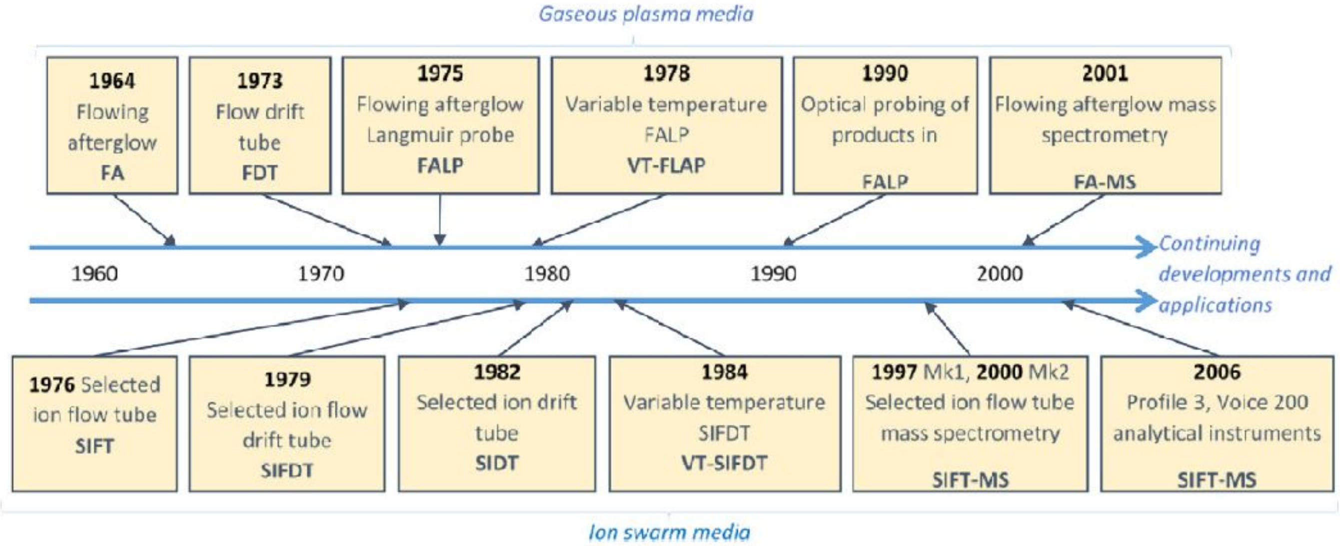

Gaseous plasma media

1964 Flowing afterglow **FA**

1973 Flow drift tube **FDT**

1975 Flowing afterglow Langmuir probe **FALP**

1978 Variable temperature FALP **VT-FLAP**

1990 Optical probing of products in **FALP**

2001 Flowing afterglow mass spectrometry **FA-MS**

1960 1970 1980 1990 2000

Continuing developments and applications

1976 Selected ion flow tube **SIFT**

1979 Selected ion flow drift tube **SIFDT**

1982 Selected ion drift tube **SIDT**

1984 Variable temperature SIFDT **VT-SIFDT**

1997 Mk1, **2000** Mk2 Selected ion flow tube mass spectrometry **SIFT-MS**

2006 Profile 3, Voice 200 analytical instruments **SIFT-MS**

Ion swarm media

Fig. 2. A timeline that indicates in the upper group the development of the flowing afterglow plasma technique, FA, and its variants, and in the lower group the selected ion flow tube, SIFT, ion swarm technique and its variants, including those with embedded electrostatic drift fields. All these techniques involve quantitative mass spectrometry as the essential diagnostic and have been vigorously exploited to study ion-molecule reactions at thermal and near-thermal energies. The inclusion of Langmuir probes into the FA created FALP instruments, which have been used to study recombination and electron attachment reactions at thermal energies. Strictly, the FDT included in the plasma group involves an ion swarm reactor that is formed by isolating ions from the gaseous plasma created in the flowing carrier gas. The latest developments see the creation of the novel selected ion flow tube mass spectrometry analytical method, SIFT-MS, by which ambient gas analysis can be realised obviating sample preparation and flowing afterglow mass spectrometry, FA-MS, for isotopic analysis of water vapour.

Flowing afterglow plasma

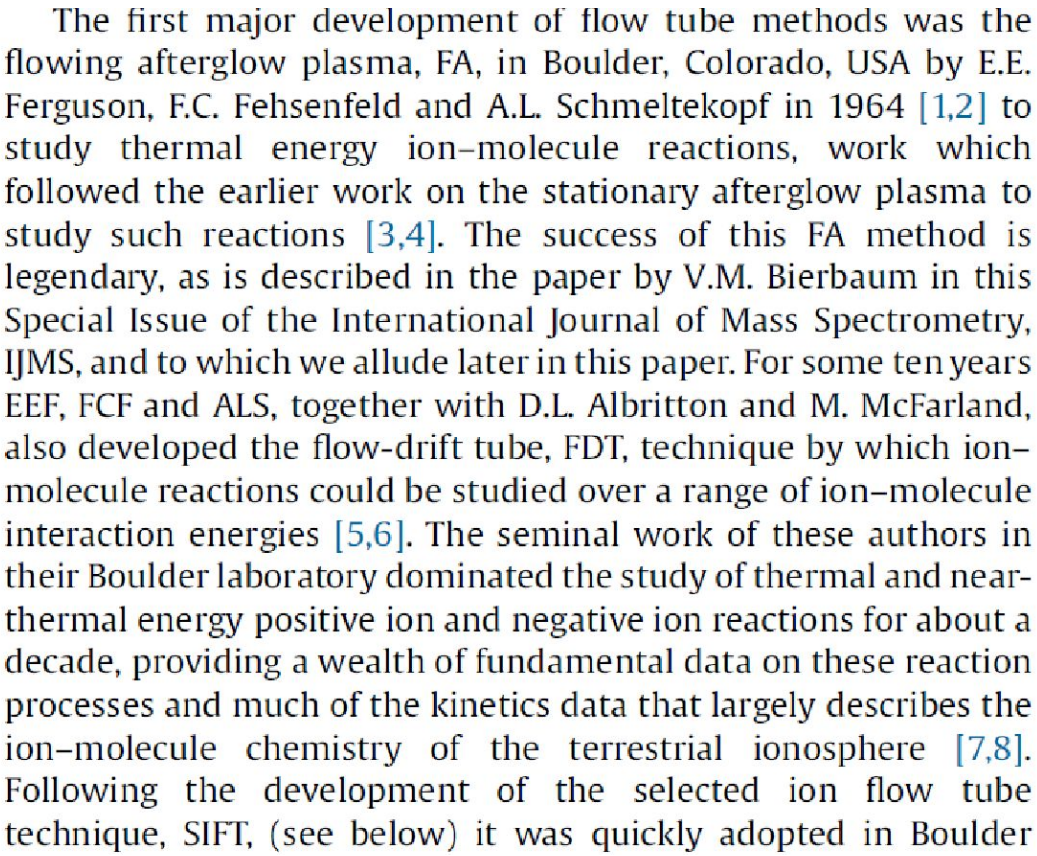

The first major development of flow tube methods was the flowing afterglow plasma, FA, in Boulder, Colorado, USA by E.E. Ferguson, F.C. Fehsenfeld and A.L. Schmeltekopf in 1964 [1,2] to study thermal energy ion–molecule reactions, work which followed the earlier work on the stationary afterglow plasma to study such reactions [3,4]. The success of this FA method is legendary, as is described in the paper by V.M. Bierbaum in this Special Issue of the International Journal of Mass Spectrometry, IJMS, and to which we allude later in this paper. For some ten years EEF, FCF and ALS, together with D.L. Albritton and M. McFarland, also developed the flow-drift tube, FDT, technique by which ion–molecule reactions could be studied over a range of ion–molecule interaction energies [5,6]. The seminal work of these authors in their Boulder laboratory dominated the study of thermal and near-thermal energy positive ion and negative ion reactions for about a decade, providing a wealth of fundamental data on these reaction processes and much of the kinetics data that largely describes the ion–molecule chemistry of the terrestrial ionosphere [7,8]. Following the development of the selected ion flow tube technique, SIFT, (see below) it was quickly adopted in Boulder

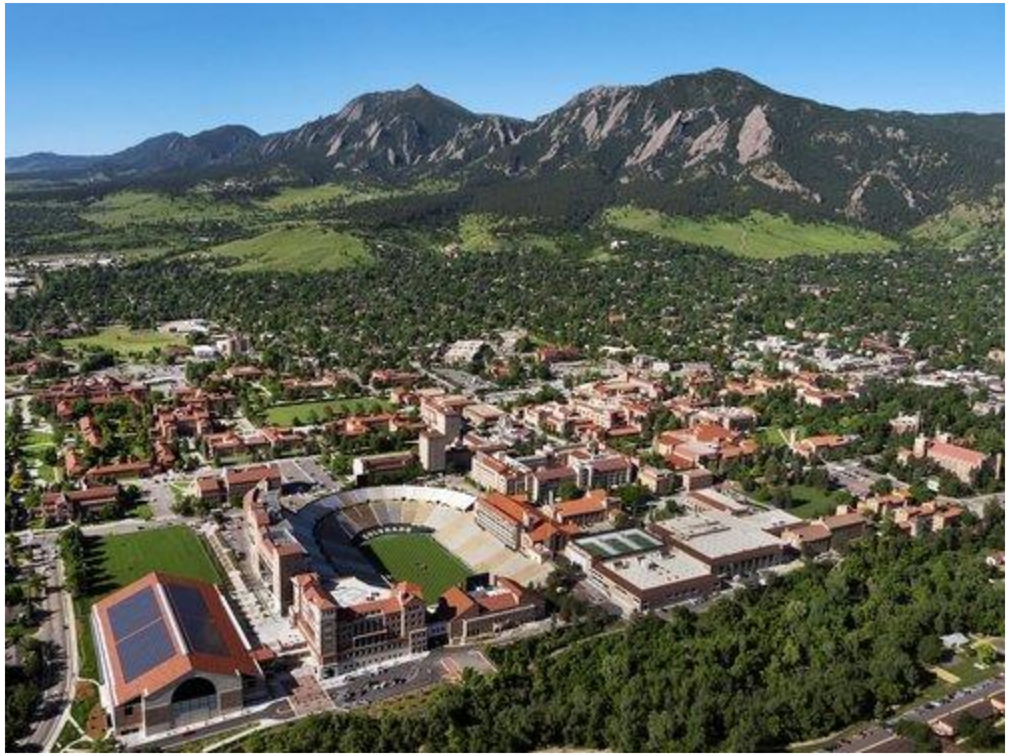

FALP, SIFT, SIFDT

FALP – Flowing Afterglow with Langmuir Probe
SIFT – Selective Ion Flow Tube
SIFDT – Selective Ion Flow Drift Tube

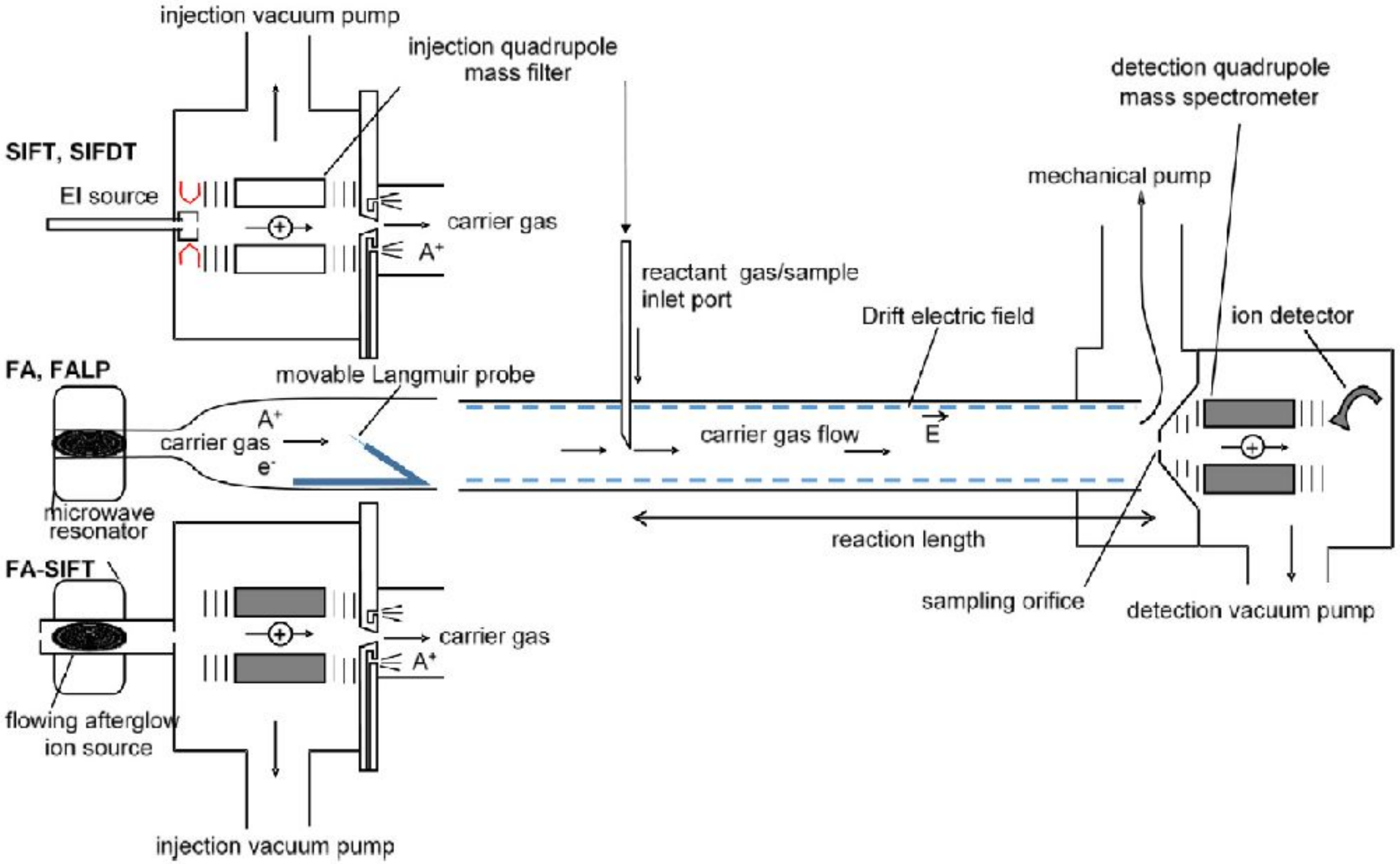

Fig. 1. Variants of flow tube systems that exploit quantitative mass spectrometry. Included are representations of the flowing afterglow, FA, and its extension to a flowing afterglow Langmuir probe, FALP, system, the selected ion flow tube, SIFT, and its extension to the selected ion flow drift tube, SIFDT, by establishing an electric field, E, along the flow tube axis, and the combination of an FA ion source with a SIFT to extend ion–molecule reaction studies to a wider variety of positive and negative ions beyond those attainable using the electron impact, EI, source and the microwave discharge source, as indicated. Implementation of variable temperature flow tubes have realised VT-SIFDT and VT-FALP instruments by which ionic and electronic reaction processes have been studied over significant temperature ranges.

FALP, SIFT, SIFDT

FALP – study of electron – ion recombination

SIFT – study of ion – molecule reactions

Measurement of ion mobility

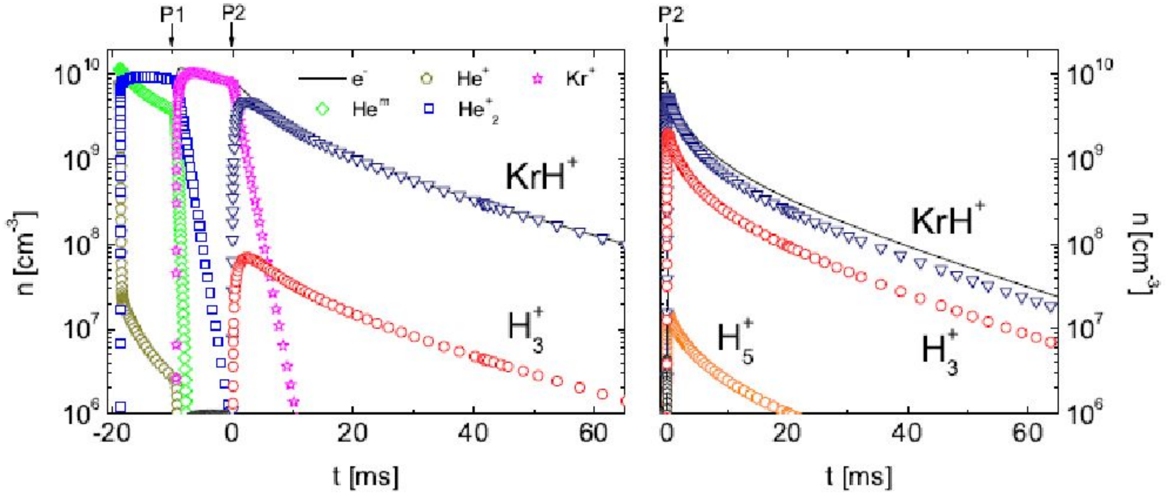

Fig. 3. Calculated ion–formation and plasma decay in the Flowing Afterglow at conditions corresponding to KrH^+ experiment. $T = 250$ K, pressure 1 600 Pa. Left panel: The plasma evolution calculated with $[Kr] = 5.5 \times 10^{13}$ cm^{-3} (introduced at P1; $t = -11$ ms) and $[H_2] = 4 \times 10^{12}$ cm^{-3} (introduced at P2; $t = 0$ ms). Right panel: The plasma evolution calculated for the same conditions as in the calculation depicted in the left panel, only hydrogen concentration was increased to $[H_2] = 1 \times 10^{14}$ cm^{-3}. For the simplicity only the recombination dominated part is plotted (after P2). The data was obtained by solving a set of partial differential equations corresponding to the set of reactions, including diffusion and recombination losses.

Cryo-FALP II

- Cryogenic Flowing Afterglow with Langmuir Probe
- Flowtube diameter – 5 cm
- He buffer gas flow ~ 2500– 6000 sccm
- Pressure ~ 200 – 2000 Pa
- Temperature range ~ 40 – 300 K

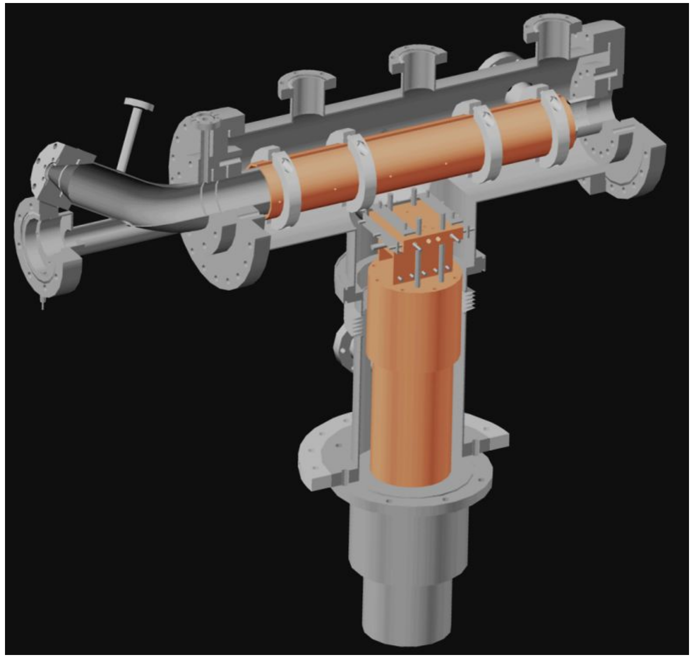

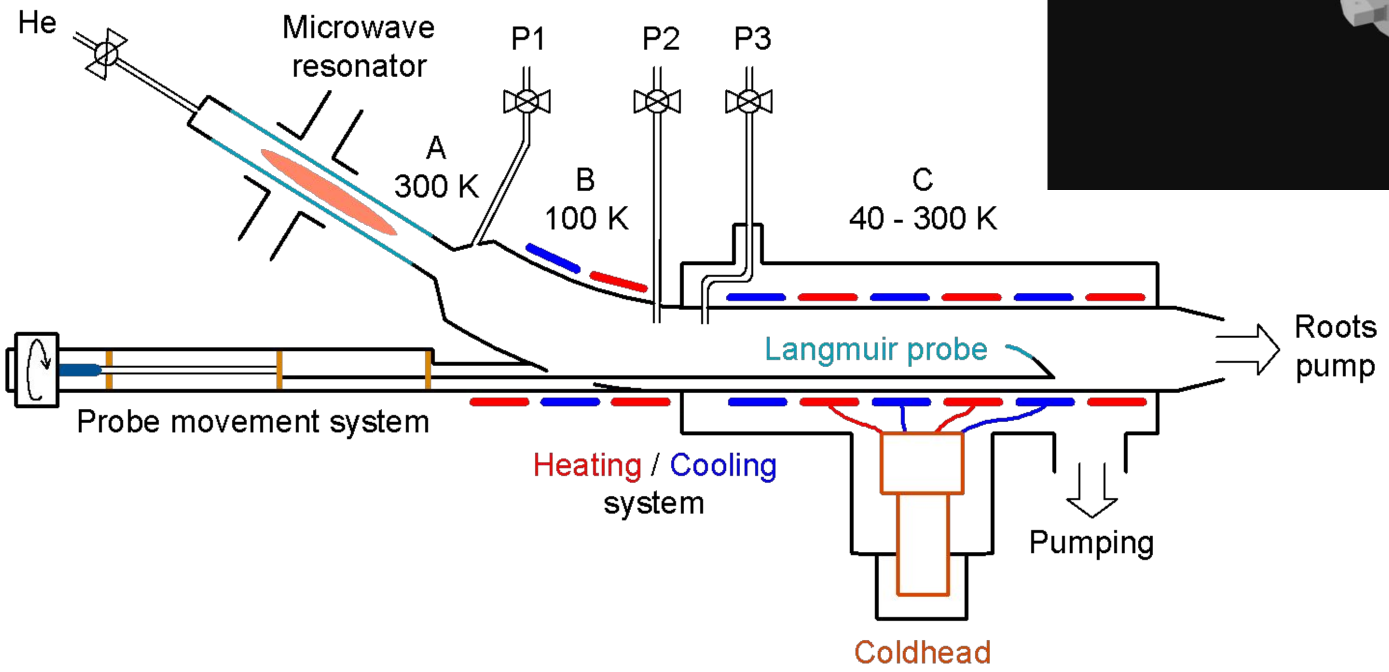

Cryo-FALP II

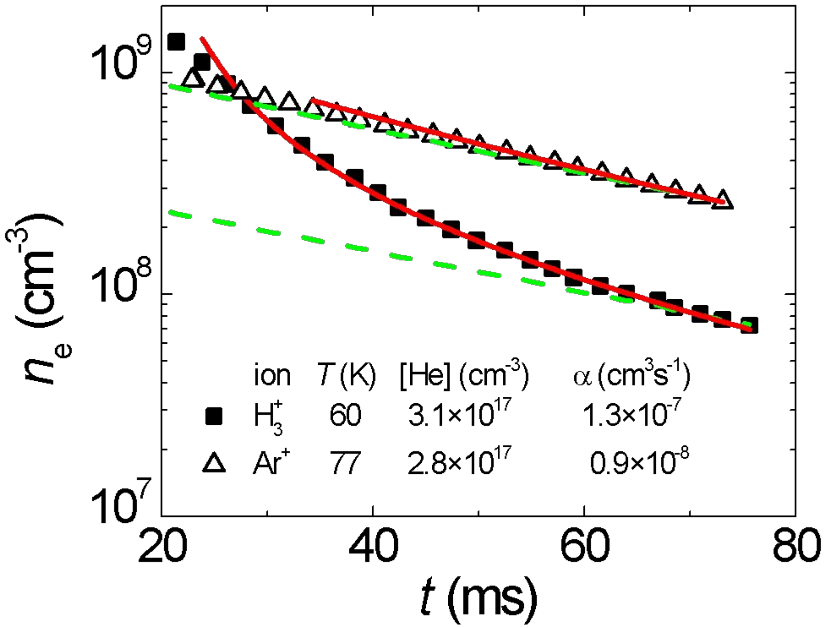

- The evolution of electron number density along the flowtube (i.e. in time) is measured
- It is possible to determine the electron energy distribution function and their temperature

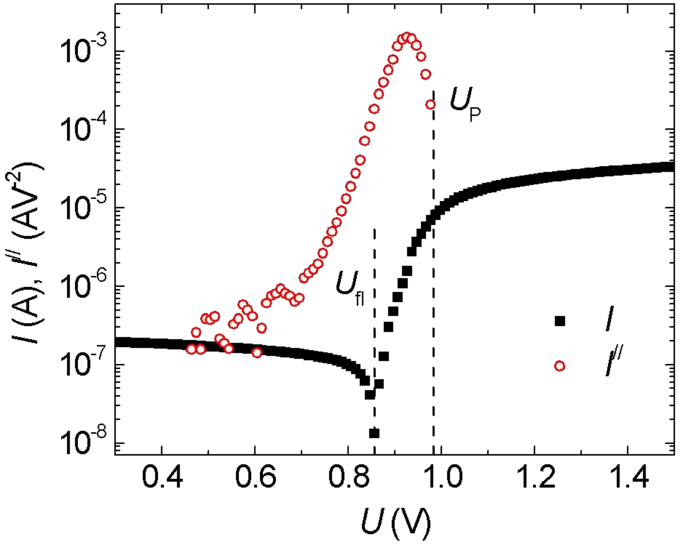

Recombination of Ar^+ ions with elekcrons, dependence on n_e

$$\mathrm{Ar}^+ + e^- + e^- \xrightarrow{K_{\text{E-CRR}}} e^- + \mathrm{Ar}$$

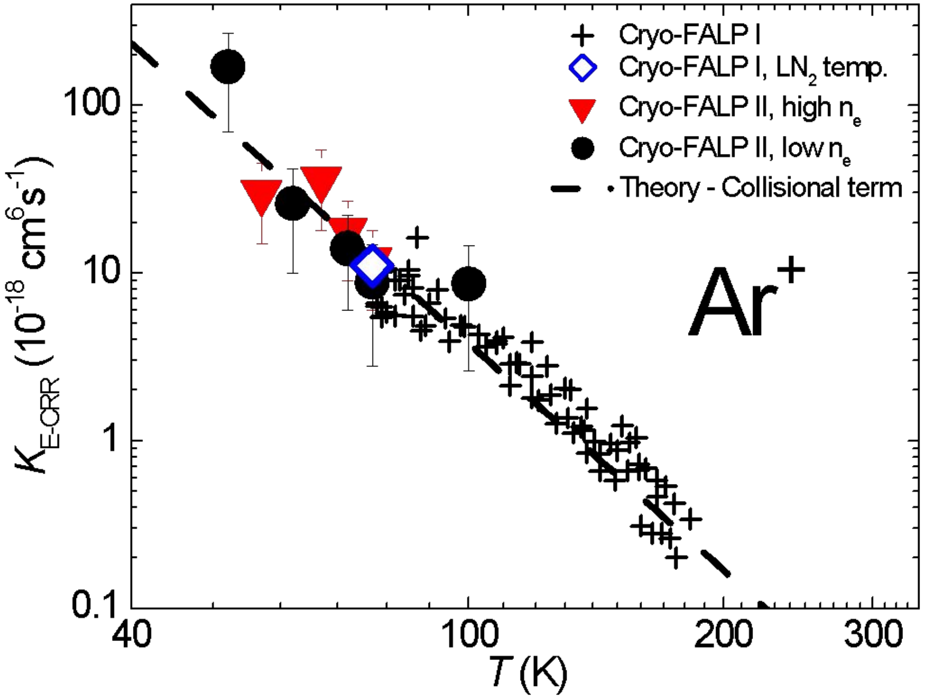

$$K_{\text{E-CRR}} = \frac{\alpha_{\text{E-CRR}}}{n_e} \cong 3.8\times10^{-9}\,T_e^{-4.5}\ \mathrm{cm^6 s^{-1}}$$

$$\frac{dn_e}{dt} = -K_{\text{E-CRR}}\,n_e^3 - \frac{1}{\tau_L}\,n_e$$

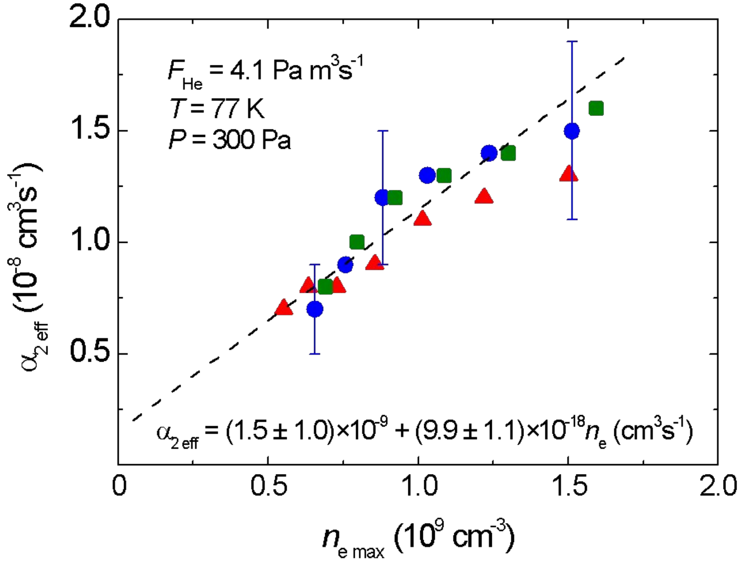

$$\alpha_{\text{eff}} = \alpha_{\text{bin}} + K_{\text{He-CRR}}[\mathrm{He}] + K_{\text{E-CRR}}\,n_e$$

Kotrík T., Dohnal P., Roučka Š., Jusko P., Plašil R., Glosík J., Johnsen R., *Phys. Rev. A* **83**, 032720, 2011.

Kotrík T., Dohnal P., Rubovič P., Plašil R., Roučka Š., Opanasiuk S., Glosík J., *Eur. Phys. J.-Appl. Phys.* **56**, 24011, 2011.

Recombination of Ar$^+$ ions with elekcrons, dependence on helium pressure

$$\mathrm{Ar}^+ + e^- + \mathrm{He} \xrightarrow{K_{\text{He-CRR}}} \mathrm{Ar} + \mathrm{He}$$

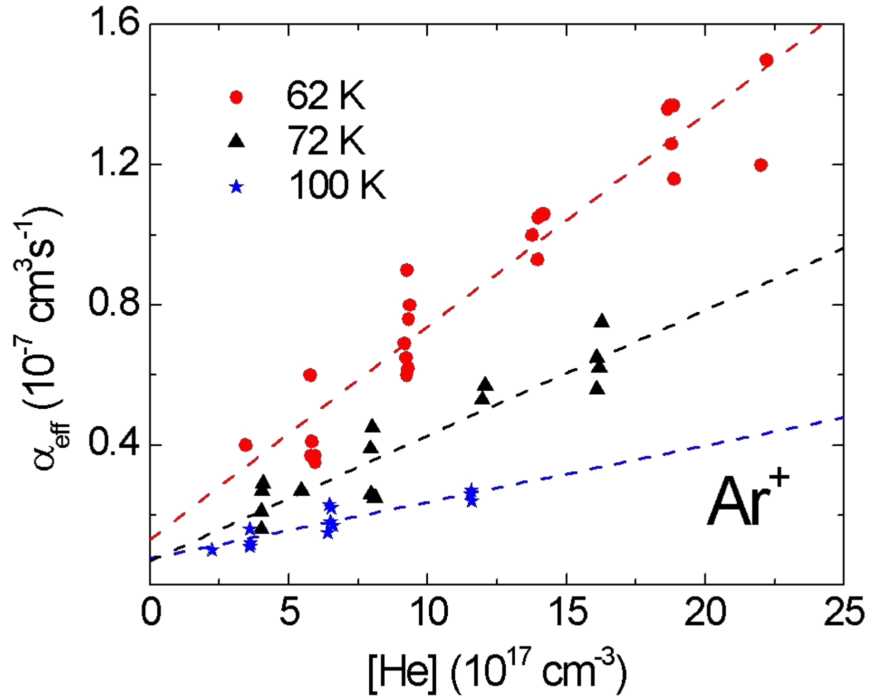

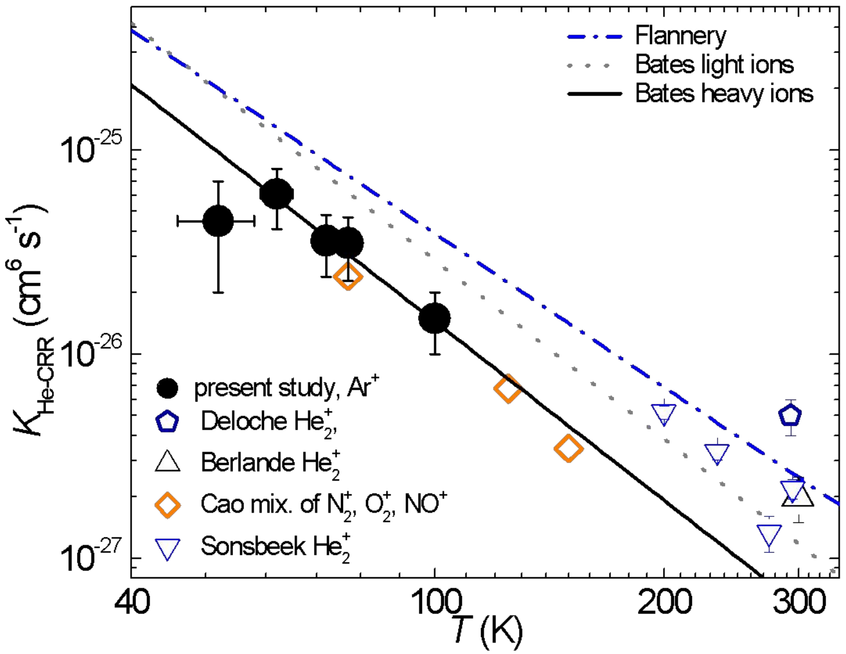

$$\alpha_{\text{eff}} = \alpha_{\text{bin}} + K_{\text{He-CRR}}[\mathrm{He}] + K_{\text{E-CRR}} n_{\text{e}}$$

Dohnal P., Rubovič P., Kotrík T., Hejduk M., Plašil R., Johnsen R., Glosík J., *Phys. Rev. A* **87**, 052716, 2013.

Calibration of Langmuir Probe

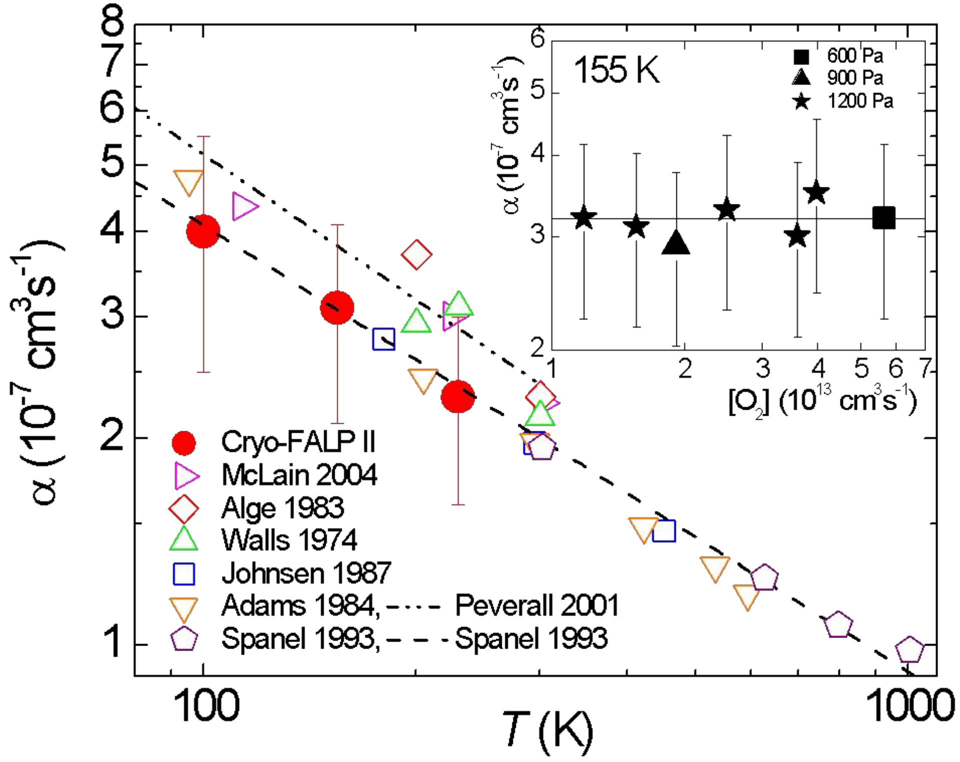

- Rekombination of O_2^+ ions with electrons is a well known process (many studies in last 50 years)
- Three body (helium assisted) recombination is at given conditions negligible
- The goal is to determine the electron number density with the best possible precision

22 rf pole ion trap

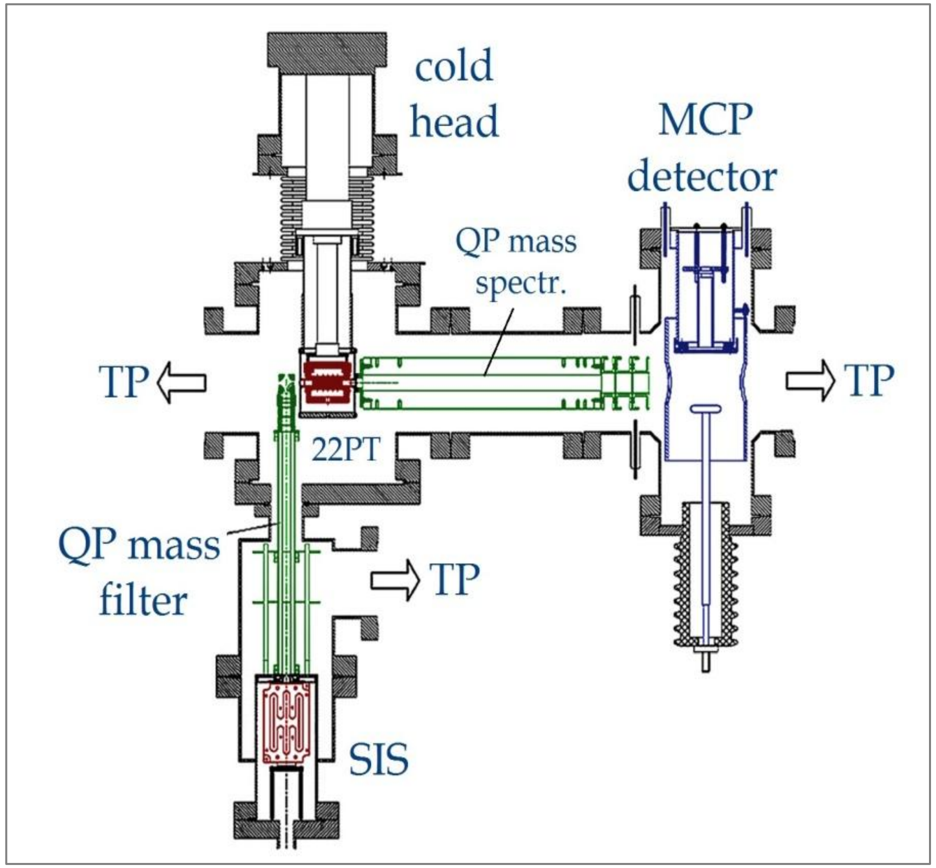

- Many configurations for different experiments
- Cold Heads at 22PT and H atom source work down to 11 K a 7 K
- Ions produced in Storage Ion Source (SIS)
- Only ions selected by QP mass filter enter the trap
- After set storage time, the ions from the trap are mass selected and detected by MCP

22 rf pole ion trap

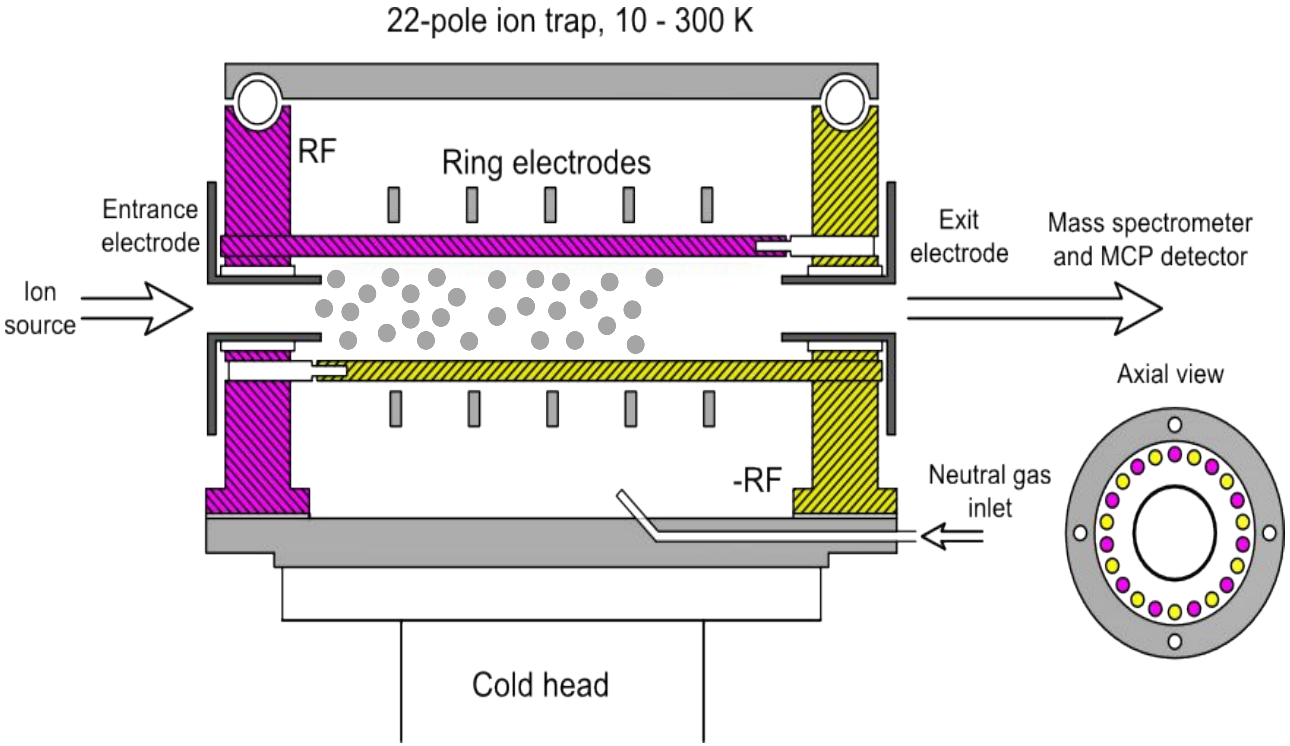

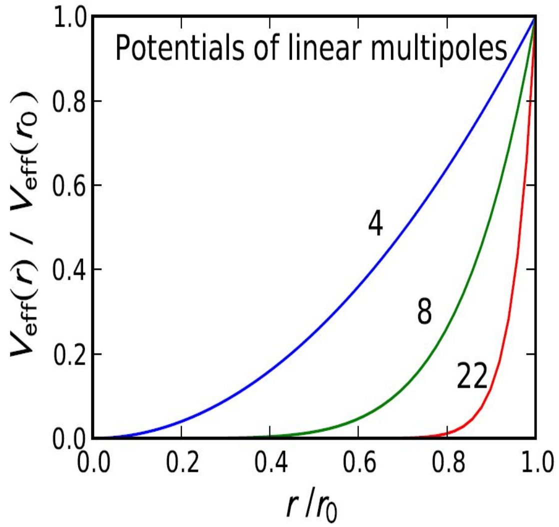

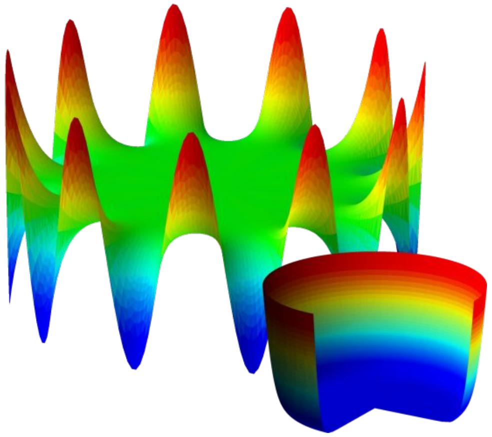

$O^- + D_2$

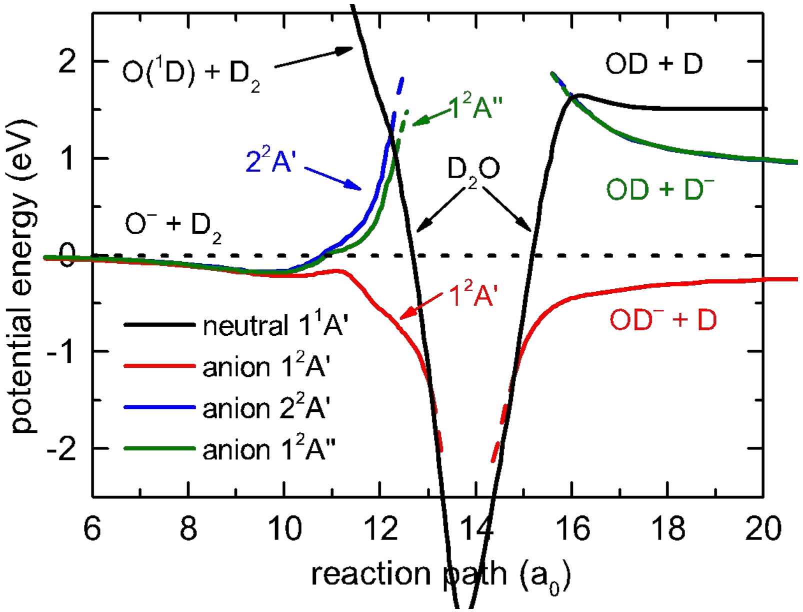

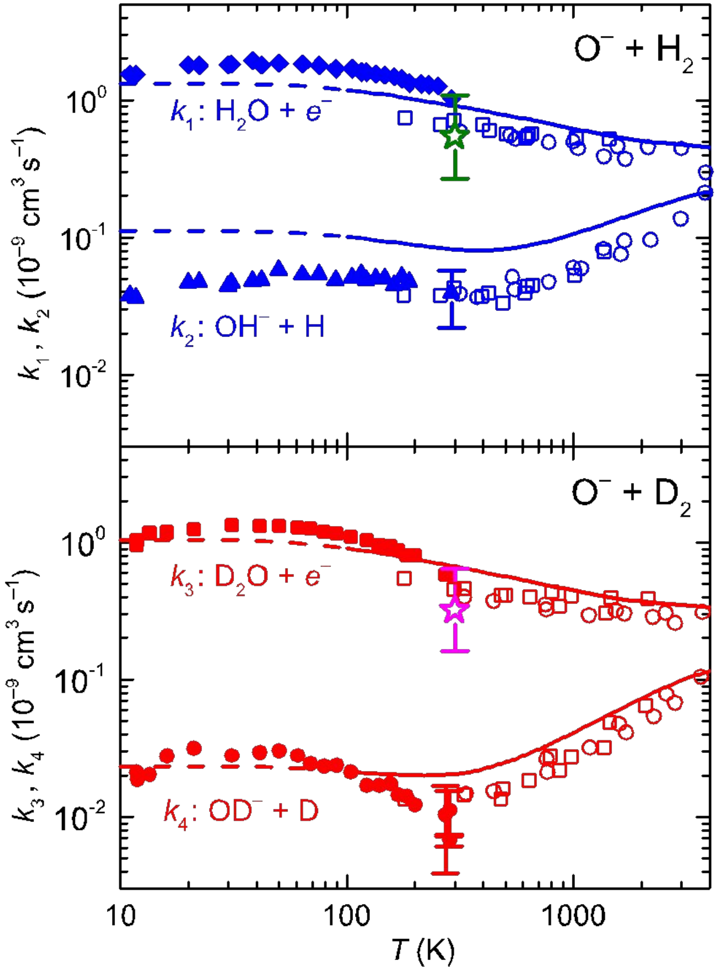

Plašil, R; Tran, TD; Roučka, Š; Jusko, P; Mulin, D; Zymak, I; Rednyk, S; Kovalenko, A; Dohnal, P; Glosík, J; Houfek, K; Táborský, J; Cížek, M, *Phys. Rev. A*, *96* (6): 062703 ,2017.

$C^{2+} + H_2$

$$C^{2+} + H_2 \rightarrow CH^+ + H^+ + 10.2\ \mathrm{eV} \tag{3a}$$

$$\rightarrow C^+ + H_2^+ + 9.0\ \mathrm{eV} \quad (C^+ + H^+ + H + 6.3\ \mathrm{eV}) \tag{3b}$$

$$\rightarrow C + H^+ + H^+ + 4.0\ \mathrm{eV} \tag{3c}$$

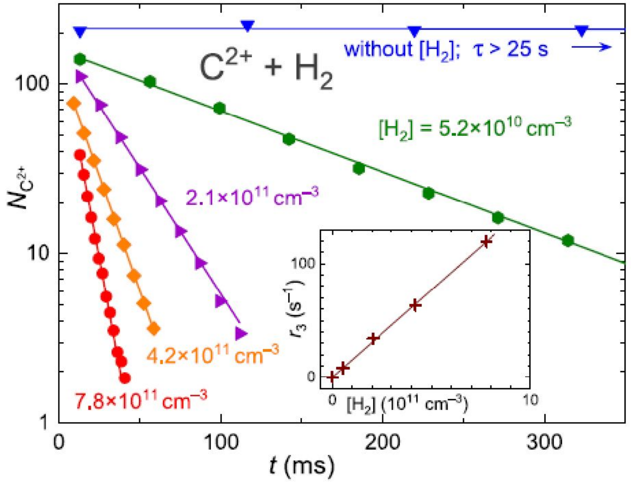

Figure 1. Time evolutions of the number of detected C^{2+} dications ($N_{C^{2+}}$) in the trap. The plotted $N_{C^{2+}}(t)$ were measured at indicated number densities of hydrogen molecules in the ion trap, at temperature $T = 22$ K and at helium number density $[\mathrm{He}] = 1.4 \times 10^{14}$ cm^{-3}. Indicated is also the decay curve measured in the He buffer without the addition of H_2 reactant gas, i.e., only the He and residual background gas from the vacuum system is present in the ion trap. The lines represent exponential fits of the individual data sets. The dependence of the obtained reaction rate r_3 vs. $[H_2]$ is shown in the inset.

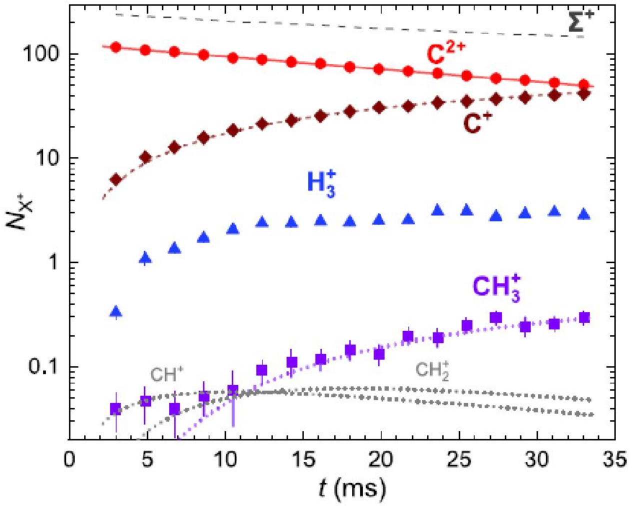

Figure 2. Time evolutions of the detected numbers of the indicated ions in the ion trap after the injection of C^{2+} dications. The plotted data were measured at $T = 39$ K, helium number density $[\mathrm{He}] = 1.8 \times 10^{13}$ cm^{-3}, and hydrogen number density $[H_2] = 1.9 \times 10^{11}$ cm^{-3}. The sum of charges Σ^+ is indicated by the black dashed line. The full line shows the fit of the exponential decrease of C^{2+} ion numbers. The dashed line shows the C^+ formation model, where 57% of C^{2+} ions are converted to C^+. The dotted lines depict the CH^+ formation model as 0.5% of the C^{2+} decrease and its two-step conversion to CH_3^+ in reactions with H_2 at the respective reaction rates (Anicich 1993). The vertical error bars represent statistical uncertainties.

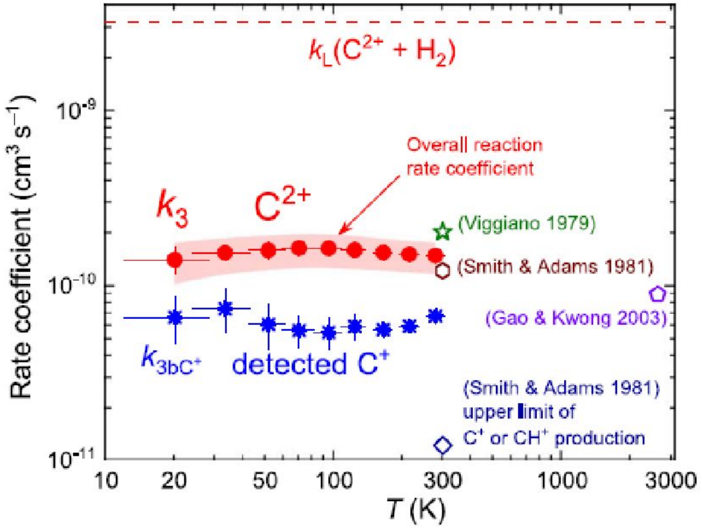

Figure 4. Temperature dependence of the reaction rate coefficient $k_3(T)$ of the reaction of C^{2+} carbon dications with H_2, comparison with previous results. The horizontal dashed line indicates the value of the Langevin collisional rate coefficient ($k_L = 3.2 \times 10^{-9}$ cm^3 s^{-1}). The circles indicate the values of $k_3(T)$ obtained in the present study for the reaction of C^{2+} carbon dications with normal H_2. The asterisks indicate values of the reaction rate coefficient $k_{3bC^+}(T)$, obtained from measured time evolutions of the number of detected C^+ ions. The values of $k_{3bC^+}(T)$ are lower limits for the actual values of rate coefficient $k_{3b}(T)$ of the reaction channel 3(b). The values of the overall reaction rate coefficient $k_3(T)$ measured with SIFT at 300 K by Smith & Adams (1981) and by Viggiano et al. (1979) are plotted as an open hexagon and an open star, respectively. The open pentagon indicates the value of the overall reaction rate coefficient $k_3(T)$ measured by Gao & Kwong (2003) at 2630 K using the cylindrical RF ion trap. The upper limit of the rate coefficient corresponding to production of C^+ and CH^+ obtained with SIFT at 300 K by Smith & Adams (1981) is plotted as an open rhomboid.

The Astrophysical Journal, 910:155 (6pp), 2021 April 1